

---

This is an electronic reprint of the original article.  
This reprint may differ from the original in pagination and typographic detail.

Chumillas, Sara; Palomäki, Tommi; Zhang, Meng; Laurila, Tomi; Climent, Victor; Feliu, Juan M.

**Analysis of catechol, 4-methylcatechol and dopamine electrochemical reactions on different substrate materials and pH conditions**

*Published in:*  
Electrochimica Acta

*DOI:*  
[10.1016/j.electacta.2018.08.113](https://doi.org/10.1016/j.electacta.2018.08.113)

Published: 01/12/2018

*Document Version*  
Peer-reviewed accepted author manuscript, also known as Final accepted manuscript or Post-print

*Published under the following license:*  
CC BY-NC-ND

*Please cite the original version:*  
Chumillas, S., Palomäki, T., Zhang, M., Laurila, T., Climent, V., & Feliu, J. M. (2018). Analysis of catechol, 4-methylcatechol and dopamine electrochemical reactions on different substrate materials and pH conditions. *Electrochimica Acta*, 292, 309-321. <https://doi.org/10.1016/j.electacta.2018.08.113>

---

This material is protected by copyright and other intellectual property rights, and duplication or sale of all or part of any of the repository collections is not permitted, except that material may be duplicated by you for your research use or educational purposes in electronic or print form. You must obtain permission for any other use. Electronic or print copies may not be offered, whether for sale or otherwise to anyone who is not an authorised user.

## **Analysis of Catechol, 4-Methylcatechol and Dopamine electrochemical reactions on different substrate materials and pH conditions.**

**Sara Chumillas<sup>a</sup>, Tommi Palomäki<sup>b</sup>, Meng Zhang<sup>c</sup> Tomi Laurila<sup>b</sup>, Victor Climent<sup>a\*</sup>, Juan M. Feliu<sup>a</sup>.**

<sup>a</sup>Instituto Universitario de Electroquímica, Universidad de Alicante, Apt. 99, 03080 Alicante, Spain

<sup>b</sup>Department of Electrical Engineering and Automation, School of Electrical Engineering, Aalto University, PO Box 13500, 00076 Aalto, Finland

<sup>c</sup>State Key Laboratory of Physical Chemistry of Solid Surfaces, Department of Chemistry, College of Chemistry & Chemical Engineering, Xiamen University, Xiamen, 361005, P.R.China

\*Corresponding author: victor.climent@ua.es, Tel.: +34 965903400

### **Abstract:**

The electrochemical behaviour of several structurally related catecholamine molecules has been investigated on different electrode materials with cyclic voltammetry, infrared spectroscopy and scanning tunneling microscopy. Emphasis was on the identification of subsequent chemical processes that follow the main electron transfer step and complicate the interpretation of the mechanism, including the polymerization reaction and fouling of the electrode surface. Among the materials investigated, gold was found out to be the most active for the oxidation of catechol, 4-methylcatechol and dopamine. At the same time, it was also the electrode least sensitive to fouling after voltammetric cycling, exhibiting the highest reversibility. The effect of pH was also investigated. Increase in pH enhanced the processes of quinone hydroxylation and polymerization. Spectroscopic measurements allowed detection of both solution and adsorbed species participating in the oxidation and polymerization processes. Finally, STM results showed the formation of polydopamine granules on gold surfaces, which grew in size as the number of cycles increased. Measured height of the granules, less than 0.5 nm, suggests a flat orientation of the molecules conforming the polymer.

**Keywords:** catecholamines; dopamine; cyclic voltammetry; in situ infrared spectroscopy; scanning tunnelling microscopy

## 1 Introduction

Intensive research in recent decades [1-3] has provided ample support for the role of quinones in biological processes, such as photosynthesis, cellular respiration and those involving signal transduction in living organisms. Quinones are magnetic molecules characterized by their ability to interact with transition metals and photons [4-6]. To this family of biological molecules belong neurotransmitters such as dopamine, adrenaline and epinephrine. There is a strong interest in the understanding of the chemistry of these molecules, and their participation in biological redox processes as well as in the devising of methods for their detection and quantification in biological fluids.

Catechol is commonly employed in several industrial processes for the production of pharmaceutical, plastic, dyes or cosmetics products [7]. Its methylated derivative is used in the production of topaquinone (trihydroxybenzene), a cofactor used by copper amine oxidases [8]. Lastly, dopamine is one of the most important neurotransmitters in human and animal bodies. The abnormal decrease of dopamine level in humans is normally related to several diseases such as Parkinson, depression or schizophrenia [9-14].

Catechol (CA), 4-methylcatechol (4-MC), 4-ethylcatechol (4-EC) and dopamine (DA) molecules possess a common structural base formed by two hydroxyl substituent groups on positions 1 and 2 of a benzene aromatic ring. While catechol does not have other substituent additional to the hydroxyl groups, 4-methylcatechol (or 4-ethylcatechol) and dopamine have a methyl (or ethyl) and an ethylamine substituent, respectively, in the position 4. In addition to the common electrochemical reactivity resulting from the shared catechol moiety, the different substituent in 4-methylcatechol and dopamine also affects their oxidation mechanisms. The substituent effect has already been studied for some naphthoquinones by using electron paramagnetic resonance (EPR) spectroscopy [15]. In addition, catechol, 4-methylcatechol and dopamine electrochemical behavior have also been deeply investigated on metallic electrodes such as platinum, gold, palladium, aluminium and copper or carbon electrodes such as graphite, glassy carbon, boron-doped diamond and tetrahedral amorphous carbon electrodes [8, 16-29]. However, there are still several fundamental questions that remain open: (i) comprehensive understanding of the electrochemical

reactions on different electrode materials is missing, (ii) adsorption behaviour of dopamine on various surfaces is not known and (iii) detailed mechanisms of the formation of passivating polydopamine films occurring on almost all types of electrode surfaces remains unsolved.

The aim of this article is to perform a comprehensive study of the electrochemical reactivity of these three compounds on different electrode materials. In this way, polycrystalline gold (Au) and platinum (Pt) metallic electrodes have been used for electrochemical characterization and their reactivity compared with a novel tetrahedral amorphous carbon (ta-C) electrode material. Given the structural differences between the three studied molecules, this paper aims to investigate and rationalize the effect of the substituent on the aromatic rings on the rate of electron transfer for each molecule. Our paper targets not only to clarify the electron transfer pathways and mechanisms that take place in the electrode-solution interphase, but also to identify the nature and morphology of electro-adsorbed species on the electrode surface. With this respect, the present study differs from those abundant in the literature on the subject, where typically one of the above aspects, but not both, has been considered. This aim has been addressed by the combined application of different techniques such as cyclic voltammetry, Fourier transform infrared reflection absorption (FTIRRAS) and attenuated total reflectance (ATR) spectroscopy and scanning tunnelling microscopy (STM). Cyclic voltammograms were recorded for the three compounds at different scan rates and pH to provide an overview of the complex electrochemical and chemical reactions taking place in the system. On the other hand, spectroscopic data provided further information on the effect of the pH, the nature of the substituent and the effect of substrate on the reactivity of these molecules. Together, these studies verify the assumptions about the existence of dopamine or dopamine-derivative adsorbed species on the different electrode surfaces. Finally, scanning tunnelling microscopy experiments provided in-depth information about the distribution of dopamine molecules on the electrode surface as well as their accumulation as a function of electrode potential cycling. Thus, the present investigation provides, for the first time, a complete view of catechol, 4-methylcatechol and dopamine oxidation reaction on different electrode materials and pH conditions.

## **2 Experimental**

Cyclic voltammetry experiments were performed using a conventional electrochemical cell composed of three electrodes. Gold and platinum polycrystalline and tetrahedral amorphous carbon electrodes were used as working electrodes, while Ag/AgCl(KCl saturated) and a gold wire were used as reference and counter electrodes, respectively. Gold and platinum electrodes were annealed in a Bunsen flame and quenched in water. Fabrication of the ta-C thin film electrodes is described in detail in [30]. ta-C electrodes were thoroughly rinsed with water before use. A  $\mu$ Autolab Type III was used for potential control. The pH 7.2 phosphate electrolyte buffer solution was prepared from  $\text{NaH}_2\text{PO}_4$  and  $\text{Na}_2\text{HPO}_4$  (Sigma-Aldrich), dissolving the appropriate quantities in ultrapure water (Ultra ElgaPurelab, 18.2  $\text{M}\Omega$  cm). Total phosphate concentration was kept equal to 0.1M. Phosphate buffer solutions (PBS) of pH 10.8 were prepared by mixing 0.05 M  $\text{Na}_2\text{HPO}_4$  and 0.1 M NaOH. Additional experiments were performed in 0.5 M  $\text{H}_2\text{SO}_4$  (pH 0.65) solution (from Merck Suprapur). Electrochemical measurements were performed in freshly prepared 1mM dopamine (Alfa Aesar, 99 %), catechol (Sigma-Aldrich), 4-methylcatechol and 4-ethylcatechol (Sigma-Aldrich) solutions. Prior to each experiment, the solution was deoxygenated during 10 or 15 minutes by bubbling argon (N50). During cyclic voltammetric measurements, oxygen presence was avoided by keeping an inert argon atmosphere over the electrolyte solution. All experiments were performed at room temperature and the pH of the electrolyte buffer solutions was measured using a Crison 507 pH meter.

Fourier transform infrared spectroscopy experiments (FTIR) were performed with a Nicolet 8700 spectrometer using a MCT detector, and a spectroelectrochemical cell with a similar configuration to the one employed for the cyclic voltammetric measurements. The bottom of the cell was provided by a  $\text{CaF}_2$  prism with a 60 degrees angle. Spectra were collected with a resolution of 8  $\text{cm}^{-1}$ , using light with both p and s polarization and plotted in absorbance mode:

$$A = -\log \frac{R_{\text{sample}}}{R_{\text{ref}}} \quad (1)$$

Spectroscopic measurements were done in both 0.1 M  $\text{HClO}_4$  (Merck Suprapur) and 0.1 M sodium phosphate buffer solutions.

Internal reflection infrared spectroscopy experiments (ATR) were performed using as working electrode a 25 nm-thick gold film deposited on a silicon prism by thermal evaporation in a vacuum chamber of a PVD75 coating system (Kurt J. Lesker Ltd.)

equipped with a turbo molecular pump. Pressure in the deposition chamber before the deposition was ca.  $10^{-6}$  Torr. The deposition rate was  $0.006 \text{ nm s}^{-1}$ , and the film thickness was monitored with a quartz crystal microbalance. ATR experiments were performed after formation of a polydopamine film by cyclic voltammetry both in the presence of deuterium oxide and under dry conditions.

STM experiments were performed with either a PicoScan (Molecular Imaging) or a Nanoscope E (Digital Instruments) scanning tunnelling microscope. In situ STM measurements were collected inside of a wood chamber, in order to avoid external vibrations that could distort the image. STM cell configuration was composed by a Au(111) single crystal as working electrode. Platinum wires served as counter and pseudo reference electrodes. The STM tips were mechanically cut Pt/Ir wires. Dopamine STM experiments were done to characterize dopamine adsorption and polymerization. Polydopamine layers were deposited by potential cycling on a Au(111) electrode immersed in a sodium phosphate buffer solution pH 7.2 containing 1 mM dopamine concentration. After dopamine deposition, the electrode was transferred to the STM chamber and the images were obtained at open circuit in air. STM image data were collected in constant height mode.

### **3 Results and discussion.**

#### **3.1 Voltammetric characterization.**

##### **Catechol and 4-methylcatechol on Pt, Au and ta-C electrodes.**

Figure 1 shows the characteristic cyclic voltammogram of a polycrystalline platinum electrode in the presence of 1 mM catechol at  $50 \text{ mVs}^{-1}$  using three solutions of different pH. In all cases, a well-defined redox couple is observed, corresponding to catechol oxidation to the corresponding orthoquinone. In the case of 4-MC, similar oxidation and reduction peaks are observed although at slightly different potential values (see Supporting Information, Figure S1). The evolution of peak height and potential with scan rate for catechol redox peaks on Pt is summarized in table 1. (Similar data for 4-MC is given in table S1). The different height of anodic and cathodic peaks and the increase of the cathodic peak as the scan rate increases agree with the existence of a chemical step after the main oxidation process. This is reflected in the values of the ratio between cathodic and anodic peak current that, in most cases,

deviates from unity, especially at pH 10.8 and low scan rates. In fact, at pH 10.8 the reduction peak is almost undetectable at scan rates below  $50 \text{ mVs}^{-1}$  for both catechol (Figure 1C) and 4-methylcatechol (Figure S1-C). For both molecules, the oxidation process is followed by either a water nucleophilic attack that generates hydroxylated species or by dimerization or polymerization reactions [31-33]. Such side reactions produce the depletion from the solution of the oxidation product (the corresponding quinone), resulting in a decrease of the corresponding cathodic peak, especially noticeable at the most alkaline pH.

Table 1 summarize the data for the change of peak potential ( $\Delta E_p$ ) with the scan rate in the case of catechol (corresponding data for 4-methylcatechol is in table S1) on platinum electrodes. These data indicates that  $\Delta E_p$  becomes larger with the increase of the scan rate for all the pH conditions. The same behaviour was observed for ta-C electrodes [34]. This indicates a quasireversible or irreversible behaviour. In all cases, the largest peak potential separation is observed in neutral pH, while smaller values for  $\Delta E_p$  are measured in both acid and alkaline solutions, evidencing the importance of pH in the catalysis of the electrochemical process. The effect of pH on the consecutive transfer of two  $\text{H}^+$  and two  $\text{e}^-$  ( $\text{QH}_2 \rightarrow \text{Q} + 2\text{H}^+ + 2\text{e}^-$ ) has been analyzed in the past using a 9 members square mechanism [35, 36]. There is an ample number of possible behaviours and pathways, depending on the relative values of pH,  $\text{p}K_i$  and intermediate rate constants. At very acidic solutions, the first electron transfer ( $\text{QH}_2 \rightarrow \text{QH}_2^+ + \text{e}^-$ ) might precede the deprotonation step, while at neutral solutions the electron transfer takes place on the deprotonated species ( $\text{QH}^-$ ), resulting on a neutral radical species that can proceed through a second deprotonation, followed by a second electron transfer. Under very alkaline conditions, a second deprotonation may antecede the first electron transfer, resulting in a  $\text{Q}^{2-}$  charged species. Similar behavior to the one reported here (faster apparent rate constant at acidic or alkaline conditions) has been reported before for the reduction of hydroquinone [35].

For both catechol and 4-MC (and it will be shown later the same behaviour for dopamine), a decrease of the peak current indicates the accumulation of blocking species on the surface of the electrode, most likely from the polymerization of the oxidation products. Both, initial current and the rate of its decrease are very sensitive to the pH of the solution (see supporting information for a plot of peak currents as a function of the number of potential cycles, figures S2 and S3). In general, higher currents are registered in alkaline pH but also higher passivation rate is observed in this case. On the contrary, the lower passivation rate is observed for the neutral pH, where the height of the peak is also lower. In general, peak currents are much lower than those predicted by Randles-Sevcik equation, indicating that the surface is already partially blocked from the beginning. Careful inspection of Figure 1 indicates that most of the decrease of peak current is due to the decrease of the overlapping current that takes place at high potentials, most likely due to the oxidation of the reaction products formed after the hydrophilic attack or the polymerization step. In this way, first cycle always features a tilted base line that gradually disappears with the increasing number of cycles.

With both catechol and 4-methylcatechol, higher scan rates and lower pH values reduce the extent of fouling of the electrodes as can be concluded from the evolution of the oxidation current as a function of these variables. The faster surface blocking at high pH indicates that the coupled chemical reactions occur to a greater extent under these experimental conditions. This is due, among other factors, to the higher amount of deprotonated species that favours the hydroxylation.

Peak separation for catechol and 4-methylcatechol also increases with potential cycling indicating that the fouling of the surface not only decreases the height of the peak, but also hinders the overall rate of the reaction. The increase in  $\Delta E_p$  is more pronounced in acidic media than in neutral or basic pH (Figure S5 and S6). Comparison of the increase of peak potential for both molecules under the same pH conditions indicate that  $\Delta E_p$  values are much lower in the case of 4-methylcatechol than for catechol. This results support the initial hypothesis described in references [37, 38], which indicate that both electron donor capacity and steric impediments, generated by the existence of a methyl side chain on the aromatic skeleton, facilitate the 4-methylcatechol oxidation

process on platinum electrodes. Regarding the steric impediments, it is possible that the methyl side chain impedes the formation of a compact adlayer of adsorbed products that decreases the rate of electron transfer as in the case of catechol.

Voltammetric peaks for catechol (Figure 2) and 4-methylcatechol (Figure S7 in supporting information) oxidation on gold are better defined and more reversible than in the case of platinum. Both the peak potential and the shift with the pH are very similar for both molecules on the two electrode materials, indicating that oxidation-reduction mechanism for both compounds is the same. As described before, part of the oxidized species is consumed in a chemical step that follows the main electron transfer, resulting in a reduction of the associated cathodic peak.

The main difference between gold and platinum is that the voltammetric profile on the former remains essentially unchanged even after prolonged cycling. This behavior, together with only a slight drop in the current density recorded at pH 10.8 suggest less fouling by catechol and 4-methylcatechol on gold than on platinum (or ta-C) electrode surfaces. As there are no drastic differences in  $I_{red}/I_{ox}$  ratios (compare tables 1 and S1 with tables S2 and S3) between the two electrode materials, especially at pH 7.2 and higher, the extent of the chemical reaction is similar for both materials (as expected for a homogeneous chemical reaction) and the different behavior is just due to a different extend in the adsorption of reaction products. While  $\Delta E_p$  for oxidation of both molecules on gold slightly increases with the scan rate in the three pH media, the main difference with platinum is that  $\Delta E_p$  on gold remain practically constant during cycling.

### **Dopamine on Pt, Au and ta-C electrodes**

Figures 3 and 4 describe the typical cyclic voltammetric profiles for platinum and gold electrodes in the presence of 1 mM dopamine. These voltammograms show a main redox process very similar to the one observed for catechol and 4-methylcatechol. In addition to the main redox couple observed at high potential, a second redox couple at lower potentials is observed for both electrodes in neutral and basic media. These voltammetric features for dopamine on platinum and gold are consistent with an electrochemical mechanism in which dopamine oxidation process at high potentials, resulting in dopamine o-quinone, is followed by a pH-dependent Michael addition reaction (in the aromatic ring positions 1 and 4), producing a cyclized product called leucodopaminechrome [39-46]. This chemical reaction is followed by a second

oxidation process, either chemical or electrochemical [47], resulting in the formation of 5, 6-dihydroxyindoline quinone (see table 2). In the cathodic scan, dopamine o-quinone reduction takes place regenerating the dopamine. Finally, the second redox pair at low potentials has been assigned to the reduction of 5, 6-dihydroxyindoline quinone (or its corresponding tautomeric compound called dopaminechrome) to form leucodopaminechrome (the relation between different tautomers is summarized in scheme S1).

Analysis of the pH dependence of the oxidation peak (as registered on the first cycle) indicates the existence of different reaction mechanisms or pathways depending on the solution pH. In the presence of dopamine, values of the oxidation current for both gold and platinum become higher as the solution pH increases (Figure 5 and 6). In fact, the positive current registered at neutral pH is approximately twice of the current registered in acid media. Similarly, the anodic peak current also increases from neutral to basic pH although in this case the recorded increase is smaller. These trends can be rationalised in agreement with Randles-Sevcik equation that predicts a value of peak current proportional to the number of transferred electrons. At low pH, the open-chain dopamine-quinones are protonated to a great extent, and the chemical-cyclization reaction is unfavorable. Under these conditions, only two electrons are transferred during the dopamine (0) oxidation to the corresponding dopaminequinone (+2). For this reason, no peaks are registered at low potential values in acid media, Figure 3 and 4 A. Meanwhile, at higher pH values, the majority of the dopamine-quinone molecules are unprotonated, thus favoring the cyclization reaction. Therefore, in neutral pH two additional electrons are generated after the chemical step in a subsequent oxidation process that gives rise to the dopaminechrome species (+4). Finally, in basic media an additional oxidation step leads to the formation of 5,6-indolequinone (+6) from dopaminechrome or its tautomeric compound 5,6-dihydroxyindole.

Similarly to what has described above for catechol and 4-MC, the ratios between anodic and cathodic peak currents for dopamine on gold and platinum are far from unity for all the scan rates, revealing the existence of coupled homogeneous reactions that can be attributed to the chemical-cyclization reaction that follows the main oxidation process [48-50].

Regarding the peak separation,  $\Delta E_p$  for dopamine on platinum and gold electrodes increases with the scan rate in acid, neutral and basic media (see tables 3 and S4). The variation of  $\Delta E_p$  with pH follow the same trends previously described for CA and 4-MC, with the highest  $\Delta E_p$  obtained at pH 7.2, followed by H<sub>2</sub>SO<sub>4</sub> and pH 10.8, respectively (at 50 mVs<sup>-1</sup> and pH 10.8 no dopamine reduction peak is detected, thus no values for dopamine  $\Delta E_p$  can be determined). A similar trend was also observed on ta-C electrodes [34]. As discussed above, this can be rationalized using the 9 member square mechanism. However, in this case the situation is more complex given the multiple tautomeric equilibriums (see scheme S1) that give place to the formation of a large number of possible reaction intermediates as a function of pH.

We describe now the time evolution of voltammetric peaks in the case of dopamine. A decrease in the oxidation peak as the number of cycles increases for all the scan rates at neutral or higher pH is seen with both Pt and Au (Figure 5 and 6). Blockage of platinum and gold surfaces proceeds faster at low scan rates and/or in solutions with high pH (Figure 5 and 6, respectively). Besides, low scan rates produce the distortion of the dopamine redox peaks giving rise to a current plateau after the peak. It has been described before that the 5,6-dihydroxyindole molecule is an intermediate in the formation of a polydopamine film, which is most likely responsible for the decrease of the peak current observed during potential cycling [51].

The time evolution of  $\Delta E_p$  can be seen in figures S5 and S6. In the case of gold, the peak potential separation ( $\Delta E_p$ ) does not change with potential cycling in acid media, whereas in neutral solutions a small increase of the peak potential separation with the number of cycles, which becomes greater with increasing the scan rate, is detected. (Trends described above for the three studied molecules, catechol, 4-methylcatechol and dopamine, as a function of scan rate and the solution pH and for the different studied electrodic materials are summarized in table S5).

### 3.2 FTIR and ATR characterization

In order to complement further the investigation on catecholamines oxidation, IR spectroscopic data were recorded as a function of the electrode potential. In situ absorbance spectra for dopamine using Pt single crystal electrodes at neutral pH conditions have been already described in [47]. However, while the emphasis in the

previous paper was to identify the nature of adsorbed species on the surface of the platinum single crystal, the present manuscript attempts a more detailed description of the products of the main oxidation reaction on the different materials and pH of the solution.

### **Catechol on Pt(111)**

To investigate the role of ethylamine substituent on the aromatic benzene structure, catechol spectroscopic behavior was recorded in acid and neutral media. Measurements in the presence of catechol were performed using a reference and a sample potential of 0.4 and 0.9 V vs RHE (reversible hydrogen electrode), respectively. The spectra shown in Figure 7 is obtained by subtracting spectra collected at 0.4 V as reference from the spectra collected at 0.9 V as sample. Thus, positive bands correspond to the products of the oxidation while negative bands to the consumption of initial catechol present on the thin layer. Figure 7A collects in situ infrared absorption spectra for Pt(111) single crystal in a 3mM catechol solution in 0.1M HClO<sub>4</sub> in D<sub>2</sub>O. Figure 7B shows the spectroscopic results in an aqueous sodium phosphate buffer solution, pH 7.2, in the presence of 20 mM catechol with the same electrode. Spectroscopic measurements in acid media were recorded in deuterium water (D<sub>2</sub>O) to avoid the HOH bending interference from water around 1600 cm<sup>-1</sup>. Similar bands are observed in both aqueous and deuterated media. Features recorded at 1516, 1473, 1414, 1375 and 1275 cm<sup>-1</sup> are detected in aqueous conditions. By contrast, in deuterated water catechol bands appear at 1504, 1457, 1414 and 1275. All the mentioned bands are observed using both p and s light. By monitoring the change of negative bands around 1516, 1473 and 1275 cm<sup>-1</sup> it is possible to follow the consumption of bulk-solution catechol species. Band at 1275 cm<sup>-1</sup> is assigned to the stretching of catechol C-OH group, while signals recorded around 1470 and 1516 cm<sup>-1</sup> correspond to the C-C bond stretching coupled to the CH ring bending mode [25, 52, 53]. Positive bands around 1650-1700 cm<sup>-1</sup> are in the region of carbonyl groups and therefore can be attributed to the formation of the quinone. Assignment of the main bands observed in the spectra for catechol oxidized and reduced species are collected in table 4.

### **Dopamine on Pt(111)**

Figure 8A shows the in-situ absorbance spectra for a Pt(111) electrode immersed in a 20 mM dopamine solution in 0.1 M HClO<sub>4</sub>, while figure B shows similar spectroscopic

results recorded at neutral pH in sodium phosphate buffer. Other experimental conditions are similar to those described above for catechol.

The main negative bands are detected at 1522, 1450, and 1289  $\text{cm}^{-1}$  both in neutral and acid media. The two at higher wavenumbers corresponds to aromatic C-C stretching while the latter corresponds to the COH stretching [54, 55]. The observation of the latter signals indicates the disappearance of OH groups due to the formation of the corresponding dopaminechrome. On the other hand, the positive band observed at 1558  $\text{cm}^{-1}$  can be assigned to the stretching of aromatic CC bonds in the oxidized molecule. Additionally, the other two positive bands at 1428 and 1321  $\text{cm}^{-1}$  are usually taken as indication of the presence of compounds with indoline structures formed after the dopamine oxidation-reduction process and the subsequent chemical reaction. These bands have been previously assigned to the  $\text{C}=\text{N}^+-\text{C}$  (1428  $\text{cm}^{-1}$ ) and C-C (1321  $\text{cm}^{-1}$ ) bonds in the indoline backbone, respectively. In this paper we propose *a new assignment for the band at 1321  $\text{cm}^{-1}$  based on both voltammetric and spectroscopic results collected at different pH conditions for dopamine behavior on Pt(111) electrodes* (Figure 5 (A, B) and Figure 8 (A, B)). The absence of a redox peak in the potential range between 0 and 0.4 V in acid conditions indicates that the cyclized product 5,6-dihydroxyindoline quinone is not formed under these conditions. This precludes the assignment of the upward band at 1321  $\text{cm}^{-1}$  to the indoline skeleton C-C stretching. Moreover, comparison of spectroscopic results for catechol and dopamine reveals the absence of the 1321  $\text{cm}^{-1}$  band in the case of catechol. For these reasons, we ascribe this band to the  $\text{CH}_2$  in-plane bending of the ethyl substituent in the hydroxylated aromatic ring structure of dopamine [56]. The observation of similar bands in the case of 4-ethylcatechol (Figure 9) support this assignment. Table 5 collects the main bands observed in the spectra for dopamine oxidized and reduced species.

### **Polydopamine formation of Au in PBS**

According to the voltammetric results presented above and STM data (see below), it is rather clear that gold electrodes are partly passivated after some voltammetric sweeps in the presence of dopamine at pH 7.2. To learn more about the polymerization process, ATR experiments were carried out on a thin gold film deposited on a silicon prism (as described in the experimental section). To form the corresponding polydopamine film

over the gold surface, a 20 mM dopamine sodium phosphate buffer solution was added into the spectroelectrochemical cell and several cycles were recorded until the complete disappearance of dopamine redox peaks. Then, the solution was removed and the polydopamine modified gold electrode was dried under argon flow. A spectrum collected with the dry gold film before polydopamine deposition was employed as reference. The resulting spectrum is shown in figure 10 while table 6 summarizes the assignment of the main bands.

Most of the bands collected in Figure 10 coincide with the bands reported for polydopamine deposited on template stripped gold electrodes [51]. These results provide further evidence that after the cycling process, a polymer film layer, mainly composed of polydopamine, passivate most of the working electrodes surface area. Positive bands around 1600 and 1450  $\text{cm}^{-1}$  correspond to the aromatic ring C=C bond stretching mode, while signals recorded at 1535 and 1374  $\text{cm}^{-1}$  wavenumbers are referred to the  $\nu_{\text{ring}}$  (C=N) and the  $\nu$  (C=N<sup>+</sup>-C), respectively. The previous assignment implies that leucodopaminochrome formed after the chemical step is oxidized in a second electron transfer process yielding the corresponding dopaminochrome. The detection of the latter two signals supports the idea of having a passivating layer integrated by aromatic compounds with amine groups and 5,6-dihydroxyindoline or 5,6-indolequinone species. A similar explanation was also given by Zangmeister et al [51]. The upward peak around 1718  $\text{cm}^{-1}$  is associated with the quinone C=O groups formed during the polymer deposition on the electrode. Spectroscopic signals around 3400 and 3300  $\text{cm}^{-1}$  are characteristic of the N-H stretching mode,  $\nu$  (N-H), of primary and secondary amine groups suggesting the existence of non-oxidized or non-cyclated dopamine molecules. Finally, bands at 2955, 2924 and 2855  $\text{cm}^{-1}$  demonstrate the existence of aliphatic carbon groups in the thin polymer layer.

Further research in this area include ATR experiments recorded in the presence of a dopamine free sodium phosphate buffer solution (Figure 11) using a -0.5 V sample potential value after formation of a polydopamine film on the electrode surface. Before measurements, blank spectra were collected at -0.5 V (vs Ag/AgCl) using both p and s polarized light, with a resolution of 8  $\text{cm}^{-1}$ . Then, dopamine in a 20 mM concentration was added into the spectroelectrochemical cell. The accumulation of (poly)dopamine on the electrode surface and its subsequent polymerization was promoted by potential cycling between 0.6 and -0.6 V until a constant oxidation current was reached. Later,

dopamine solution was removed and replaced with fresh sodium phosphate buffer solution.

In this case, dopamine polymer shows only one main band at  $1228\text{ cm}^{-1}$ . This band is recorded only with p light, suggesting its assignment to adsorbed species. The  $1228\text{ cm}^{-1}$  band is assigned to the out-of-plane deformation of C-O-C with p- $\pi$  conjugation and its detection signals the formation of a polyindole thin film [57-59]. The spectrum collected with s-polarized light shows one negative band at  $1450\text{ cm}^{-1}$ . Negative bands correspond to species present at the reference potential and therefore cannot be assigned to dopamine related products. Most likely this band is due to the interference of partially deuterated water molecules. Absence of clear positive bands in the spectrum with s polarized light suggest that no dopamine molecules are dissolved back into the fresh buffer from the passivating film.

### 3.3 STM-Dopamine characterization

Figure 12 A shows an STM image of the unreconstructed Au(111)-(1x1) annealed surface. Au(111) image exhibits large and well-defined terraces separated by different monoatomic steps [60, 61]. Figures 12(B-D), (E-H) and (I-K) collect different Au(111) STM images for dopamine modified gold surface after an increasing number of voltammetric adsorption cycles, using scan sizes of  $200\times 200$ ,  $100\times 100$  and  $50\times 50\text{ nm}^2$ , respectively.

Images show deposited dopamine or dopamine derivatives on Au(111) electrode after different cyclic voltammetric experiments (Figure S8 in supporting information summarize the electrochemical experiments with the STM sample in a conventional electrochemical cell). Comparison of gold blank and gold-dopamine images after the voltammetric experiment, demonstrates that many bright spots appear over the electrode surface after the cycling process. Those bright spots are attributed to the patches of adsorbed molecules over the electrode surface after dopamine electrochemical polymerization process. According to the images, the increase of the number of cycles also increases the spot size. Interestingly, the spots are regularly distributed on the surface leaving significant portions uncovered. However, we cannot discard from this image the existence of a continuous film of one or few monolayers covering the whole surface above which the polymer ‘granules’ grow. Moreover, these

STM results are also corroborated by dopamine ATR experiments in dry conditions, where the formation of a polydopamine film on gold electrodes after the electrochemical absorption process was clearly demonstrated.

Table 7 summarizes heights and sizes of the clusters depending on the number of voltammetric cycles carried out. Comparison of the average height values of the spots with typical values of distances in  $\pi$ - $\pi$  stacking of aromatic molecules [62] suggests that molecules lie flat on the surface and thickness of the polymer layer is no more than two or three layers.

Finally, as gold showed least amount of fouling in CV experiments it can be expected that the formation of these types of structures would be more extensive on platinum and ta-C electrode surfaces.

#### 4 Conclusions

Voltammetric results described above demonstrate that, among the different materials tested, gold is the electrode that experiences the least intensive fouling process during or after potential cycling in the presence of catechol, 4-methylcatechol and dopamine. Therefore, we conclude that gold is also the most active electrode material towards the oxidation of these three compounds. Moreover, comparison of the gold voltammetric profiles with those obtained using platinum or ta-C electrodes indicates that peaks are better defined and clearer in the first case. From the voltammetric analysis it can be concluded that the lower  $\Delta E_p$  is also obtained on gold substrates suggesting a higher “reversibility” for those redox processes on gold in comparison with platinum or ta-C electrodes. In glassy carbon (GC), which is among the more common materials employed for catecholamine electroanalytical investigation, the electron transfer rate is faster for all the studied molecules in comparison with Pt or ta-C. However, comparing GC with Au, reaction rate is faster on Au for CA and MC, while similar rate is observed for DA. Moreover, as pointed out previously [36, 63], reaction rate on GC is very dependent on the exact chemical nature of the electrode surface and therefore this behaviour may depend on the pretreatment of the electrode. On the other hand, the chemical nature of the electrode surfaces employed in this study is well known and perfectly reproducible. Another important conclusion is that, as a general trend, rate of

reaction for the three molecules investigated is faster in acid or alkaline solutions, in comparison with the neutral pH.

Spectroscopy results on gold films allow characterizing both the solution and the adsorbed species on or near the electrode surface for each molecule and support the existence of a dopamine or dopamine-derivative adsorption layer that cover most of the electrode active area as was indicated by the voltammetric results. Careful comparison of voltammetric and spectroscopic data of the related molecules catechol, 4-ethylcatechol and dopamine leads us to reconsider the assignment of one of the bands in the spectra of oxidised dopamine. Further, STM results provided the direct visual proof that after potential cycling in the presence of 1 mM dopamine neutral solution, different molecules become adsorbed on the surface since several spots, randomly distributed over the electrode surface are observed. In addition, spot sizes are higher as the number of cycles recorded becomes higher. Thus, an increase of the number of cycles produces a decrease in the available electrode area. Finally, this manuscript clearly points out the synergy of cyclic voltammetry, infrared spectroscopy and STM experiments. In this way, the electrode fouling indicated (for all the studied molecules) by the cyclic voltammetry technique (with the numbers of cycles) has been also proved by the spectroscopic characterization and in case of dopamine by the STM imaging of the polydopamine layer extended on the electrode surface.

## **5. Acknowledgements:**

The authors thankfully acknowledge financial support from the UA-FPU 2013-5796 grant, the Ministerio de Economía, Industria y Competitividad (CTQ2016-76221-P), the European Framework Program-Marie Curie Actions under the ELECTRONANOMAT Project (Grant No. PIRSES-GA-2012-318990) and Academy of Finland (Project Number #285526)

## **6. References**

- [1] R.N. Adams, Probing Brain Chemistry with Electroanalytical Techniques, *Anal. Chem.*, 48 (1976) 1126-8.
- [2] J.P. Allen, J.C. Williams, Photosynthetic reaction centers, *FEBS Lett.*, 438 (1998) 5-9.
- [3] D.L. Robinson, A. Hermans, A.T. Seipel, R.M. Wightman, Monitoring rapid chemical communication in the brain, *Chem. Rev.*, 108 (2008) 2554-2584.

- [4] K. Kataoka, S. Kimura, F. Shirakawa, Y. Sasaki, Studies on the Complex Formation between o -Quinones and Metal Chlorides in Nitromethane Solution, *Bull. Chem. Soc. Jpn.*, 54 (1981) 2237-2242.
- [5] L.A. Eriksson, F. Himo, P.E.M. Siegbahn, G.T. Babcock, Electronic and magnetic properties of neutral and charged quinone and plastoquinone radicals, *J. Phys. Chem. A*, 101 (1997) 9496-9504.
- [6] L. Kathawate, Y. Shinde, R. Yadav, S. Salunke-Gawali, Thermal, magnetic and spectral properties of metal quinone complexes Part IV. Alkali metal complexes of 3-chloro-2-hydroxy-1,4-naphthoquinone Synthesis characterization and thermal studies, *J. Therm. Anal. Calorim.*, 111 (2013) 1003-1011.
- [7] B. Nasr, G. Abdellatif, P. Canizares, C. Saez, J. Lobato, M.A. Rodrigo, Electrochemical oxidation of hydroquinone, resorcinol, and catechol on boron-doped diamond anodes, *Environ. Sci. Technol.*, 39 (2005) 7234-7239.
- [8] G. Li, H. Zhang, F. Sader, N. Vadhavkar, D. Njus, Oxidation of 4-Methylcatechol: Implications for the Oxidation of Catecholamines, *Biochemistry*, 46 (2007) 6978-6983.
- [9] R.M. Wightman, L.J. May, A.C. Michael, Detection of Dopamine Dynamics in the Brain, *Anal. Chem.*, 60 (1988) A769-&.
- [10] K.T. Kawagoe, R.M. Wightman, Characterization of amperometry for in vivo measurement of dopamine dynamics in the rat brain, *Talanta*, 41 (1994) 865-874.
- [11] A. Pezzella, M. dlschia, A. Napolitano, G. Misuraca, G. Prota, Iron-mediated generation of the neurotoxin 6-hydroxydopamine quinone by reaction of fatty acid hydroperoxides with dopamine: A possible contributory mechanism for neuronal degeneration in Parkinson's disease, *J. Med. Chem.*, 40 (1997) 2211-2216.
- [12] P.-Y. Ge, Y. Du, J.-J. Xu, H.-Y. Chen, Selective detection of dopamine based on the unique property of gold nanofilm, *J. Electroanal. Chem.*, 633 (2009) 182-186.
- [13] D.P. Quan, D.P. Tuyen, T.D. Lam, P.T.N. Tram, N.H. Binh, P.H. Viet, Electrochemically selective determination of dopamine in the presence of ascorbic and uric acids on the surface of the modified Nafion/single wall carbon nanotube/poly(3-methylthiophene) glassy carbon electrodes, *Colloids and Surfaces B: Biointerfaces*, 88 (2011) 764-770.
- [14] F. Micheli, Recent Advances in the Development of Dopamine D-3 Receptor Antagonists: a Medicinal Chemistry Perspective, *ChemMedChem*, 6 (2011) 1152-1162.
- [15] C.S. Coates, J. Ziegler, K. Manz, J. Good, B. Kang, S. Milikisiyants, R. Chatterjee, S.J. Hao, J.H. Golbeck, K.V. Lakshmi, The Structure and Function of Quinones in Biological Solar Energy Transduction: A Cyclic Voltammetry, EPR, and Hyperfine Sub-Level Correlation (HYSCORE) Spectroscopy Study of Model Naphthoquinones, *J. Phys. Chem. B*, 117 (2013) 7210-7220.
- [16] M.R. Deakin, R.M. Wightman, The kinetics of some substituted catechol/o-quinone couples at a carbon paste electrode, *J. Electroanal. Chem.*, 206 (1986) 167-177.
- [17] C.D. Allred, R.L. McCreery, Adsorption of catechols on fractured glassy carbon electrode surfaces, *Anal. Chem.*, 64 (1992) 444-448.
- [18] F. Malem, D. Mandler, Self-Assembled Monolayers in Electroanalytical Chemistry - Application of Omega-Mercapto Carboxylic-Acid Monolayers for the Electrochemical Detection of Dopamine in the Presence of a High-Concentration of Ascorbic-Acid, *Anal. Chem.*, 65 (1993) 37-41.
- [19] S.L. Iverson, L.Q. Hu, V. Vukomanovic, J.L. Bolton, The Influence of the p-Alkyl Substituent on the Isomerization of o-Quinones to p-Quinone Methides: Potential Bioactivation Mechanism for Catechols, *Chem. Res. Toxicol.*, 8 (1995) 537-544.
- [20] K. Miyazaki, G. Matsumoto, M. Yamada, S. Yasui, H. Kaneko, Simultaneous voltammetric measurement of nitrite ion, dopamine, serotonin with ascorbic acid on the GRC electrode, *Electrochim. Acta*, 44 (1999) 3809-3820.
- [21] S.H. DuVall, R.L. McCreery, Control of Catechol and Hydroquinone Electron-Transfer Kinetics on Native and Modified Glassy Carbon Electrodes, *Anal. Chem.*, 71 (1999) 4594-4602.

- [22] P. Ramesh, G.S. Suresh, S. Sampath, Selective determination of dopamine using unmodified, exfoliated graphite electrodes, *J. Electroanal. Chem.*, 561 (2004) 173-180.
- [23] H. Razmi, A. Azadbakht, Electrochemical characteristics of dopamine oxidation at palladium hexacyanoferrate film, electroless plated on aluminum electrode, *Electrochim. Acta*, 50 (2005) 2193-2201.
- [24] M.A. Ghanem, Electrocatalytic activity and simultaneous determination of catechol and hydroquinone at mesoporous platinum electrode, *Electrochem. Commun.*, 9 (2007) 2501-2506.
- [25] M. Rodríguez-López, A. Rodes, A. Berna, V. Climent, E. Herrero, P. Tunon, J.M. Feliu, A. Aldaz, A. Carrasquillo, Model system for the study of 2D phase transitions and supramolecular interactions at electrified interfaces: Hydrogen-assisted reductive desorption of catechol-derived adlayers from Pt(111) single-crystal electrodes, *Langmuir*, 24 (2008) 3551-3561.
- [26] T. Kondo, Y. Niwano, A. Tamura, J. Imai, K. Honda, Y. Einaga, D.A. Tryk, A. Fujishima, T. Kawai, Enhanced electrochemical response in oxidative differential pulse voltammetry of dopamine in the presence of ascorbic acid at carboxyl-terminated boron-doped diamond electrodes, *Electrochim. Acta*, 54 (2009) 2312-2319.
- [27] E.A. Khudaish, M.R. Al Birikei, The role of bromine adlayer at palladium electrode in the electrochemical oxidation of dopamine in alkaline solution, *J. Electroanal. Chem.*, 650 (2010) 68-74.
- [28] E.A. Khudaish, A.A.A. Farsi, Electrochemical oxidation of dopamine and ascorbic acid at a palladium electrode modified with in situ fabricated iodine-adlayer in alkaline solution, *Talanta*, 80 (2010) 1919-1925.
- [29] D.N. Oko, S. Garbarino, J.M. Zhang, Z.M. Xu, M.H. Chaker, D.L. Ma, D. Guay, A.C. Tavares, Dopamine and ascorbic acid electro-oxidation on Au, AuPt and Pt nanoparticles prepared by pulse laser ablation in water, *Electrochim. Acta*, 159 (2015) 174-183.
- [30] T. Laurila, V. Protopopova, S. Rhode, S. Sainio, T. Palomaki, M. Moram, J.M. Feliu, J. Koskinen, New electrochemically improved tetrahedral amorphous carbon films for biological applications, *Diamond Relat. Mater.*, 49 (2014) 62-71.
- [31] L. Papouchado, G. Petrie, R.N. Adams, Anodic-Oxidation Pathways of Phenolic Compounds .1. Anodic Hydroxylation Reactions, *J. Electroanal. Chem.*, 38 (1972) 389-+.
- [32] M.D. Ryan, A. Yueh, W.Y. Chen, The Electrochemical Oxidation of Substituted Catechols, *J. Electrochem. Soc.*, 127 (1980) 1489-1495.
- [33] G.E. Cabaniss, A.A. Diamantis, W.R. Murphy, R.W. Linton, T.J. Meyer, Electrocatalysis of Proton-Coupled Electron-Transfer Reactions at Glassy-Carbon Electrodes, *J. Am. Chem. Soc.*, 107 (1985) 1845-1853.
- [34] T. Palomaki, S. Chumillas, S. Sainio, V. Protopopova, M. Kauppila, J. Koskinen, V. Climent, J.M. Feliu, T. Laurila, Electrochemical reactions of catechol, methylcatechol and dopamine at tetrahedral amorphous carbon (ta-C) thin film electrodes, *Diamond Relat. Mater.*, 59 (2015) 30-39.
- [35] E. Laviron, Electrochemical Reactions with Protonations at Equilibrium .10. The Kinetics of the Para-Benzoquinone Hydroquinone Couple on a Platinum-Electrode, *J. Electroanal. Chem.*, 164 (1984) 213-227.
- [36] M.R. Deakin, P.M. Kovach, K.J. Stutts, R.M. Wightman, Heterogeneous Mechanisms of the Oxidation of Catechols and Ascorbic-Acid at Carbon Electrodes, *Anal. Chem.*, 58 (1986) 1474-1480.
- [37] S. Steenken, P. Oneill, Oxidative Demethoxylation of Methoxylated Phenols and Hydroxybenzoic Acids by Oh Radical - Insitu Electron-Spin Resonance, Conductometric Pulse-Radiolysis, and Product Analysis Study, *J. Phys. Chem.*, 81 (1977) 505-508.
- [38] S. Steenken, P. Neta, One-Electron Redox Potentials of Phenols - Hydroxyphenols and Aminophenols and Related-Compounds of Biological Interest, *J. Phys. Chem.*, 86 (1982) 3661-3667.

- [39] M.D. Hawley, S.V. Tatawawadi, S. Piekarski, R.N. Adams, Electrochemical Studies of the Oxidation Pathways of Catecholamines, *J. Am. Chem. Soc.*, 89 (1967) 447-450.
- [40] D.C.S. Tse, R.L. Mccreery, R.N. Adams, Potential Oxidative Pathways of Brain Catecholamines, *J. Med. Chem.*, 19 (1976) 37-40.
- [41] C.G. Chavdarian, D. Karashima, N. Castagnoli, H.K. Hundley, Oxidative and cardiovascular studies on natural and synthetic catecholamines, *J. Med. Chem.*, 21 (1978) 548-554.
- [42] T.E. Young, B.W. Babbitt, Electrochemical Study of the Oxidation of Alpha-Methyldopamine, Alpha-Methylnoradrenaline, and Dopamine, *J. Org. Chem.*, 48 (1983) 562-566.
- [43] F. Zhang, G. Dryhurst, Oxidation Chemistry of Dopamine - Possible Insights into the Age-Dependent Loss of Dopaminergic Nigrostriatal Neurons, *Bioorg. Chem.*, 21 (1993) 392-410.
- [44] X.L. Wen, Y.H. Jia, Z.L. Liu, Micellar effects on the electrochemistry of dopamine and its selective detection in the presence of ascorbic acid, *Talanta*, 50 (1999) 1027-1033.
- [45] L. Xiang, Y.Q. Lin, P. Yu, L. Su, L.Q. Mao, Laccase-catalyzed oxidation and intramolecular cyclization of dopamine: A new method for selective determination of dopamine with laccase/carbon nanotube-based electrochemical biosensors, *Electrochim. Acta*, 52 (2007) 4144-4152.
- [46] S. Corona-Avendano, G. Alarcon-Angeles, M.T. Ramirez-Silva, G. Rosquete-Pina, M. Romero-Romo, M. Palomar-Pardave, On the electrochemistry of dopamine in aqueous solution. Part I: The role of [SDS] on the voltammetric behavior of dopamine on a carbon paste electrode, *J. Electroanal. Chem.*, 609 (2007) 17-26.
- [47] S. Chumillas, M.C. Figueiredo, V. Climent, J.M. Feliu, Study of dopamine reactivity on platinum single crystal electrode surfaces, *Electrochim. Acta*, 109 (2013) 577-586.
- [48] P.E. Whitson, H.W. VandenBorn, D.H. Evans, Acquisition and analysis of cyclic voltammetric data, *Anal. Chem.*, 45 (1973) 1298-1306.
- [49] R.J. Lawson, J.T. Maloy, Mechanistic studies using double potential step chronoamperometry. EC, ECE, and second-order dimerization mechanisms, *Anal. Chem.*, 46 (1974) 559-562.
- [50] A.J. Bard, L.R. Faulkner, *Electrochemical Methods. Fundamental and Applications*, 2nd ed., John Wiley & Sons, Inc., New York, 2001.
- [51] R.A. Zangmeister, T.A. Morris, M.J. Tarlov, Characterization of Polydopamine Thin Films Deposited at Short Times by Autoxidation of Dopamine, *Langmuir*, 29 (2013) 8619-8628.
- [52] D.A. Stern, G.N. Salaita, F. Lu, J.W. Mccargar, N. Batina, D.G. Frank, L. Lagurendavidson, C.H. Lin, N. Walton, J.Y. Gui, A.T. Hubbard, Studies of L-Dopa and Related-Compounds Adsorbed from Aqueous-Solutions at Pt(100) and Pt(111) - Electron Energy-Loss Spectroscopy, Auger-Spectroscopy, and Electrochemistry, *Langmuir*, 4 (1988) 711-722.
- [53] T. Lana-Villarreal, A. Rodes, J.M. Perez, R. Gomez, A spectroscopic and electrochemical approach to the study of the interactions and photoinduced electron transfer between catechol and anatase nanoparticles in aqueous solution, *J. Am. Chem. Soc.*, 127 (2005) 12601-12611.
- [54] X.Y. Wang, B.K. Jin, X.Q. Lin, In-situ FTIR spectroelectrochemical study of dopamine at a glassy carbon electrode in a neutral solution, *Anal. Sci.*, 18 (2002) 931-933.
- [55] S. Gunasekaran, R.T. Kumar, S. Ponnusamy, Vibrational spectra and normal coordinate analysis of adrenaline and dopamine, *Indian J. Pure Appl. Phys.*, 45 (2007) 884-892.
- [56] A. Lagutschenkov, J. Langer, G. Berden, J. Oomens, O. Dopfer, Infrared spectra of protonated neurotransmitters: dopamine, *Phys. Chem. Chem. Phys.*, 13 (2011) 2815-2823.
- [57] A. Pullman, B. Pullman, The band structure of melanins, *Biochim. Biophys. Acta*, 54 (1961) 384-385.
- [58] D.S. Galvão, M.J. Caldas, Polymerization of 5,6-indolequinone: A view into the band structure of melanins, *J. Chem. Phys.*, 88 (1988) 4088-4091.

- [59] Y. Li, M. Liu, C. Xiang, Q. Xie, S. Yao, Electrochemical quartz crystal microbalance study on growth and property of the polymer deposit at gold electrodes during oxidation of dopamine in aqueous solutions, *Thin Solid Films*, 497 (2006) 270-278.
- [60] Q.J. Xie, Y.Y. Zhang, C.H. Xiang, J.X. Tang, Y.L. Li, Q.X. Zhao, S.Z. Yao, A comparative study on the viscoelasticity and morphology of polyaniline films galvanostatically grown on bare and 4-aminothiophenol-modified gold electrodes using an electrochemical quartz crystal impedance system and SEM, *Anal. Sci.*, 17 (2001) 613-620.
- [61] M.H. Holzle, T. Wandlowski, D.M. Kolb, Structural Transitions in Uracil Adlayers on Gold Single-Crystal Electrodes, *Surf. Sci.*, 335 (1995) 281-290.
- [62] M. Swart, T. van der Wijst, C. Fonseca Guerra, F.M. Bickelhaupt,  $\pi$ - $\pi$  stacking tackled with density functional theory, *Journal of Molecular Modeling*, 13 (2007) 1245-1257.
- [63] Q. Lin, Q. Li, C. Batchelor-McAuley, R.G. Compton, Two-Electron, Two-Proton Oxidation of Catechol: Kinetics and Apparent Catalysis, *J. Phys. Chem. c*, 119 (2015) 1489-1495.

Figure Captions:

**Figure 1.** Cyclic voltammetric behavior of CA on Pt in H<sub>2</sub>SO<sub>4</sub> pH 0.65(A), sodium PBS pH 7.2 (B) and pH 10.8 (C) at 50 mVs<sup>-1</sup>.

**Figure 2.** Cyclic voltammetric behavior for CA on Au in H<sub>2</sub>SO<sub>4</sub> pH 0.65 (A), sodium PBS pH 7.2 (B) and pH 10.8 (C) at 50 mVs<sup>-1</sup>.

**Figure 3.** Cyclic voltammetric behavior for DA on Pt in H<sub>2</sub>SO<sub>4</sub> pH 0.65 (A), sodium PBS pH 7.2 (B) and pH 10.8 (C) at 50 mVs<sup>-1</sup>.

**Figure 4.** Cyclic voltammetric behavior for DA on Au in H<sub>2</sub>SO<sub>4</sub> pH 0.65 (A), sodium PBS pH 7.2 (B) and pH 10.8 (C) at 50 mVs<sup>-1</sup>.

**Figure 5.** Cyclic voltammetric behavior of DA on Pt in H<sub>2</sub>SO<sub>4</sub>, sodium PBS pH 7.2 and pH 10.8 at 100 mVs<sup>-1</sup> (A, B, C) and 10 mVs<sup>-1</sup> (D,E,F).

**Figure 6.** Cyclic voltammetric behavior of DA on Au in H<sub>2</sub>SO<sub>4</sub> pH 0.65, sodium PBS pH 7.2 and pH 10.8 at 100 mVs<sup>-1</sup> (A, B, C) and 10 mVs<sup>-1</sup> (D, E, F).

**Figure 7.** In situ absorbance spectra obtained for a Pt(111) electrode immersed in A) 3 mM CA + 0.1 M HClO<sub>4</sub> solution in deuterium oxide water (D<sub>2</sub>O) and B) 20 mM CA aqueous 0.1 sodium PBS pH 7.2.  $E_{ref} = 0.4$  and  $E_{sample} = 0.9$  V. 200 interferograms were collected at each potential with a resolution of 8 cm<sup>-1</sup> and p or s polarized light.

**Figure 8.** In situ absorbance spectra obtained for a Pt(111) electrode immersed in a 20 mM DA aqueous: A) 0.1M HClO<sub>4</sub> and B) sodium PBS pH 7.2.  $E_{ref} = 0.4$  and  $E_{sample} = 0.9$ V. 200 interferograms were collected at each potential with a resolution of 8 cm<sup>-1</sup> and p or s polarized light.

**Figure 9.** In situ absorbance spectra obtained for a Pt(111) electrode immersed in a 20 mM 4-EC aqueous 0.1 sodium PBS pH 7.2.  $E_{ref} = 0.4$  and  $E_{sample} = 0.9$ V. 200 interferograms were collected at each potential with a resolution of 8 cm<sup>-1</sup> and p or s polarized light.

**Figure 10.** ATR of polydopamine adsorbed on a thin gold layer after potential cycling in a dopamine solution at pH 7.2, in dry conditions, 100 scans and 8 cm<sup>-1</sup>. Spectra were collected with p-polarized light.

**Figure 11.** ATR of DA adsorbed on a thin gold layer after cycling in a sodium PBS (D<sub>2</sub>O) containing, 100 scans and 8 cm<sup>-1</sup>. p-polarized and s- polarized light, as indicated.

**Figure 12.** STM images of adsorbed DA or DA-derivative molecules over Au(111) in air under open circuit conditions. A) Au(111)-(1x1) substrate prior to dopamine adsorption. Scan Size: 100 x 100 nm<sup>2</sup>. B) to D) Scan size: 200 x 200 nm<sup>2</sup>: B) 2 cycles. C) 10 cycles and D) 50 cycles.. E) to H) Scan size: 100 x 100 nm<sup>2</sup>: E) 2 cycles. F) 10 cycles G) 25 cycles and H) 40 cycles. I) to K) Scan size: 50 x 50 nm<sup>2</sup> I) 2 cycles. J) 10 cycles and K) 25 cycles.  $E_{bias}$  100 mV.  $I_{setpoint}$ : 800 pA.

## List of Tables

**Table 1.** Peak potential separation ( $\Delta E_p$ ) and peak current ratio ( $I_{red}/I_{ox}$ ) for 1 mM catechol (CA) in  $H_2SO_4$  (pH 0.65), sodium PBS pH 7.2 and 10.8 on Pt electrodes.

**Table 2.** Chemical structure of different oxidation products of DA

**Table 3.** Peak potential separation ( $\Delta E_p$ ) and peak current ratio ( $I_{red}/I_{ox}$ ) for 1 mM DA in  $H_2SO_4$  (pH 0.65), sodium PBS pH 7.2 and 10.8 on Pt electrodes.

**Table 4:** Assignment of the main bands observed in the spectra for catechol in the oxidized and reduced state

**Table 5:** Assignment of the main bands observed in the spectra for dopamine in the oxidised and reduced state

**Table 6.** ATR bands of polydopamine deposited on a thin-gold layer electrode.

**Table 7.** Average size and height of the spots observed in the STM image of adsorbed DA derivatives as a function of the number of voltammetric cycles.

**Figures:**

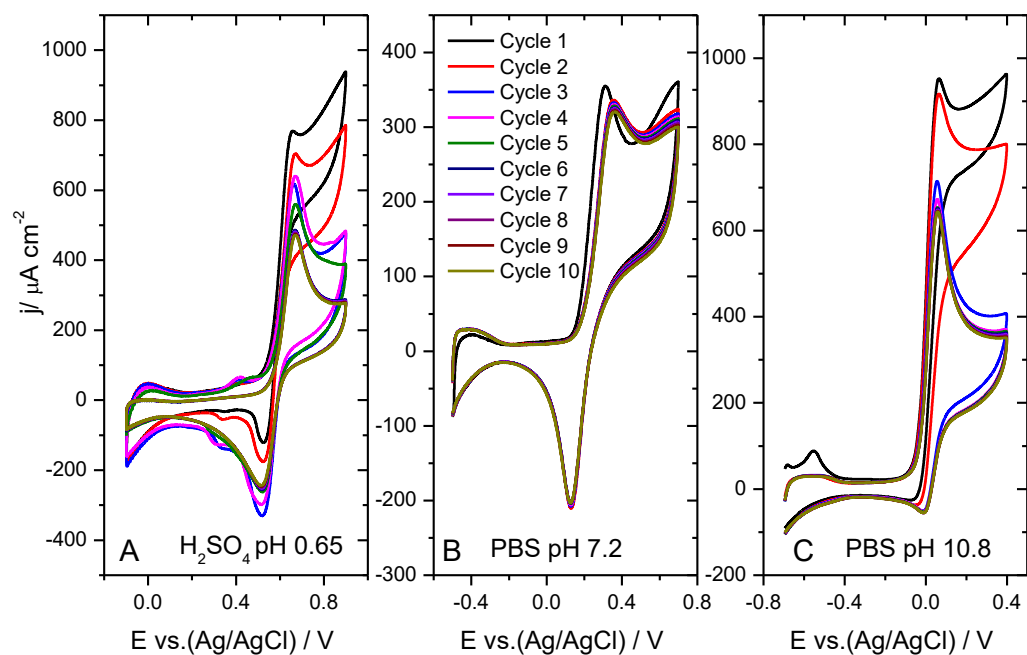


**Figure 1.** Cyclic voltammetric behavior of CA on Pt in  $\text{H}_2\text{SO}_4$  pH 0.65(A), sodium PBS pH 7.2 (B) and pH 10.8 (C) at  $50 \text{ mVs}^{-1}$ .

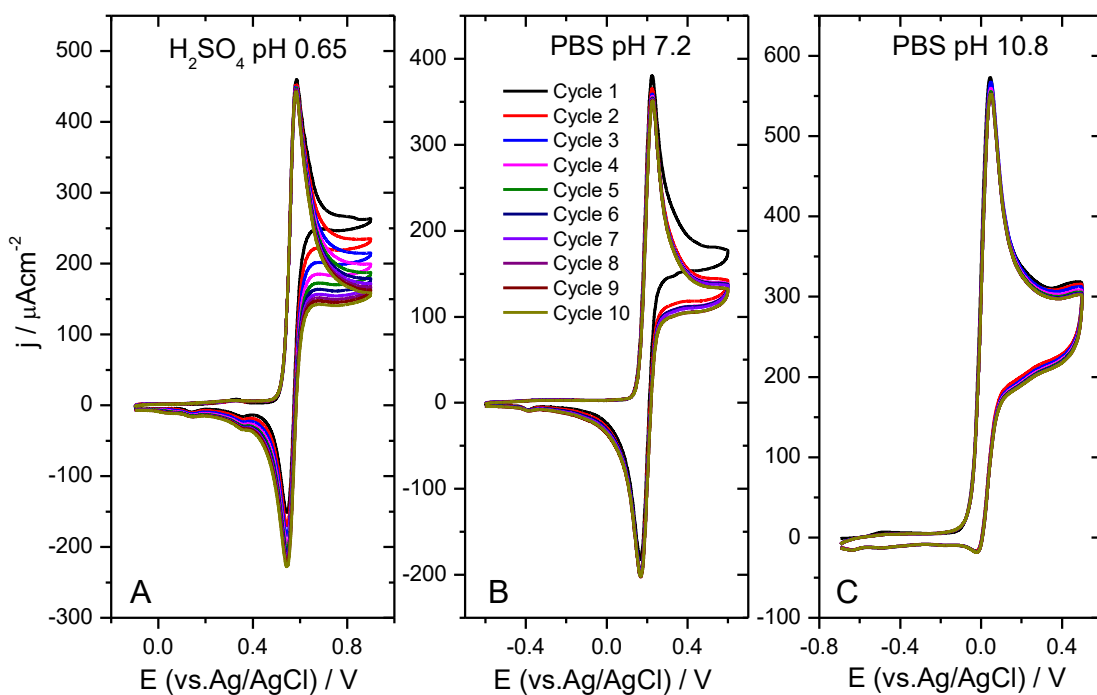


**Figure 2.** Cyclic voltammetric behavior for CA on Au in  $\text{H}_2\text{SO}_4$  pH 0.65 (A), sodium PBS pH 7.2 (B) and pH 10.8 (C) at  $50 \text{ mVs}^{-1}$ .

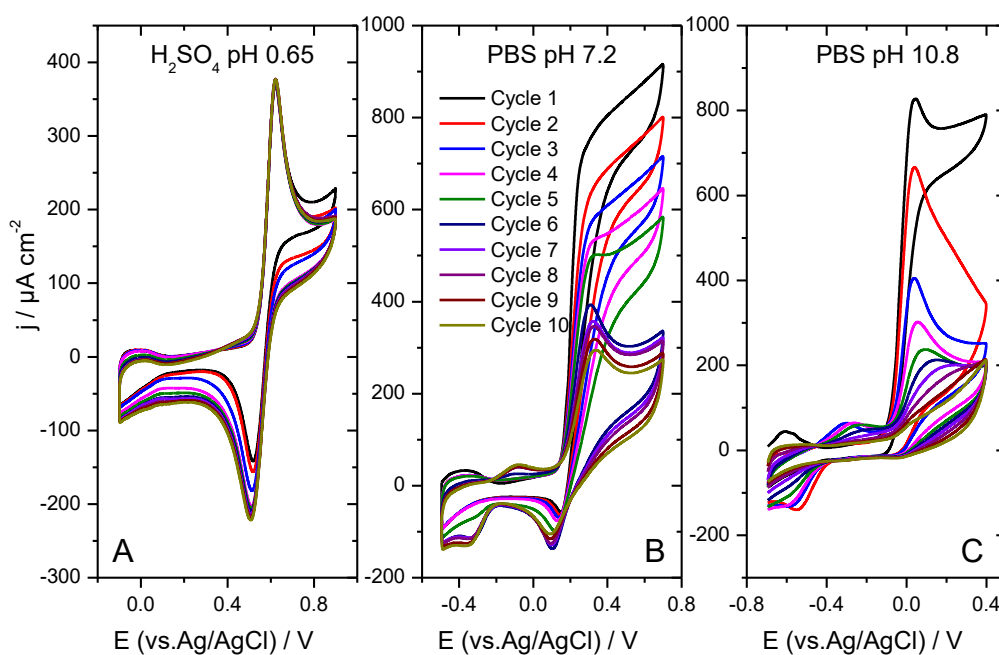


**Figure 3.** Cyclic voltammetric behavior for DA on Pt in H<sub>2</sub>SO<sub>4</sub> pH 0.65 (A), sodium PBS pH 7.2 (B) and pH 10.8 (C) at 50 mVs<sup>-1</sup>.

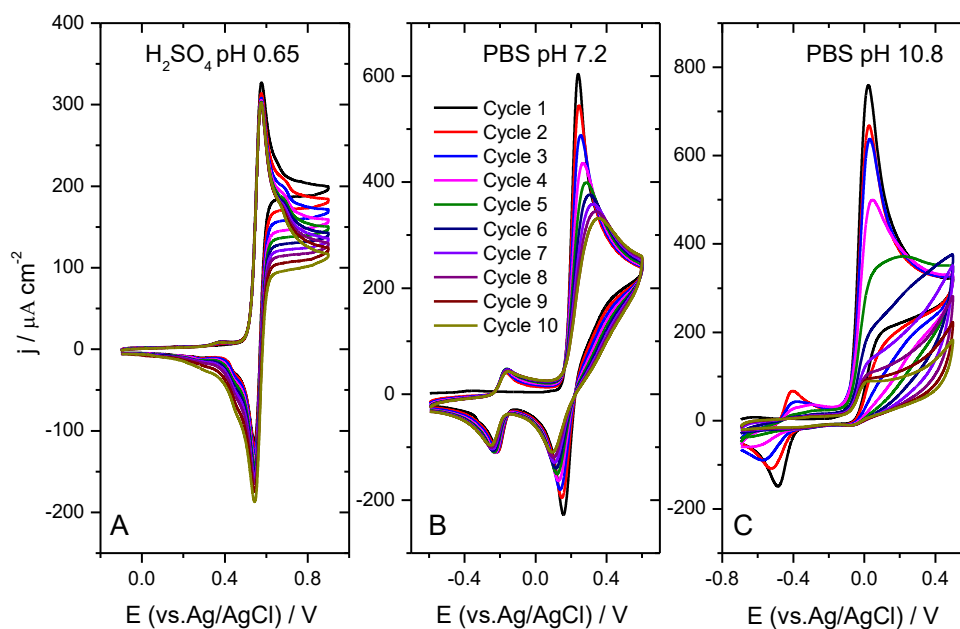


**Figure 4.** Cyclic voltammetric behavior for DA on Au in H<sub>2</sub>SO<sub>4</sub> pH 0.65 (A), sodium PBS pH 7.2 (B) and pH 10.8 (C) at 50 mVs<sup>-1</sup>.

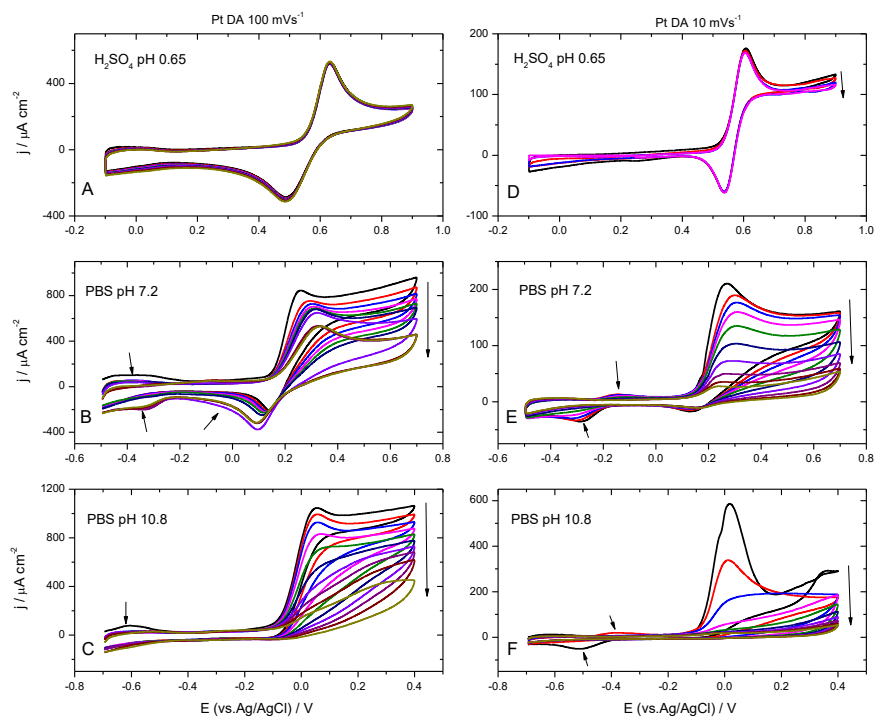


**Figure 5.** Cyclic voltammetric behavior of DA on Pt in  $\text{H}_2\text{SO}_4$ , sodium PBS pH 7.2 and pH 10.8 at  $100 \text{ mVs}^{-1}$  (A, B, C) and  $10 \text{ mVs}^{-1}$  (D,E,F).

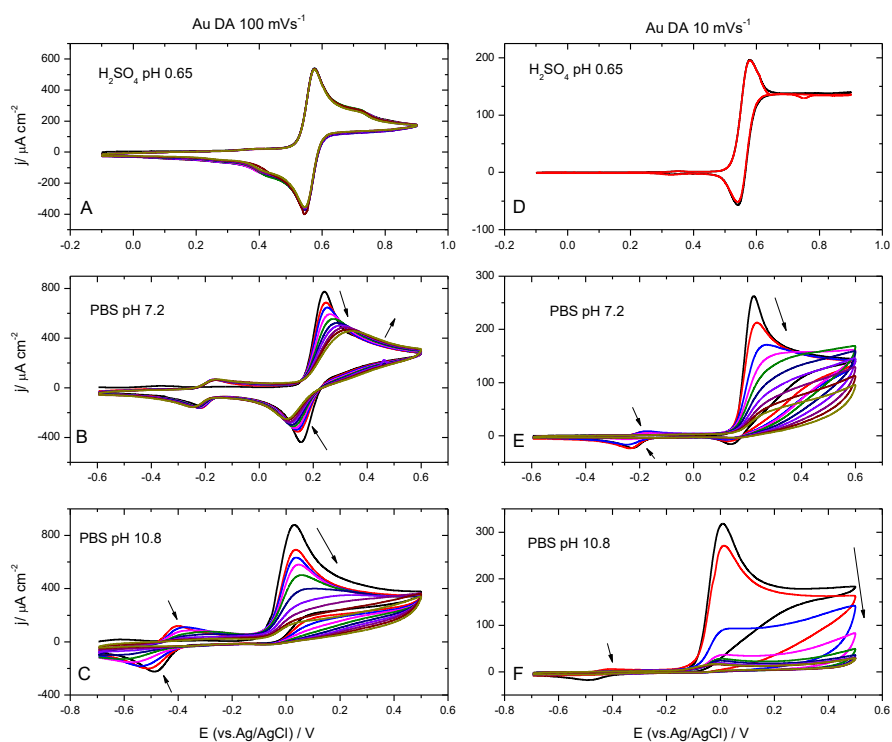


**Figure 6.** Cyclic voltammetric behavior of DA on Au in H<sub>2</sub>SO<sub>4</sub> pH 0.65, sodium PBS pH 7.2 and pH 10.8 at 100 mVs<sup>-1</sup> (A, B, C) and 10 mVs<sup>-1</sup> (D, E, F).

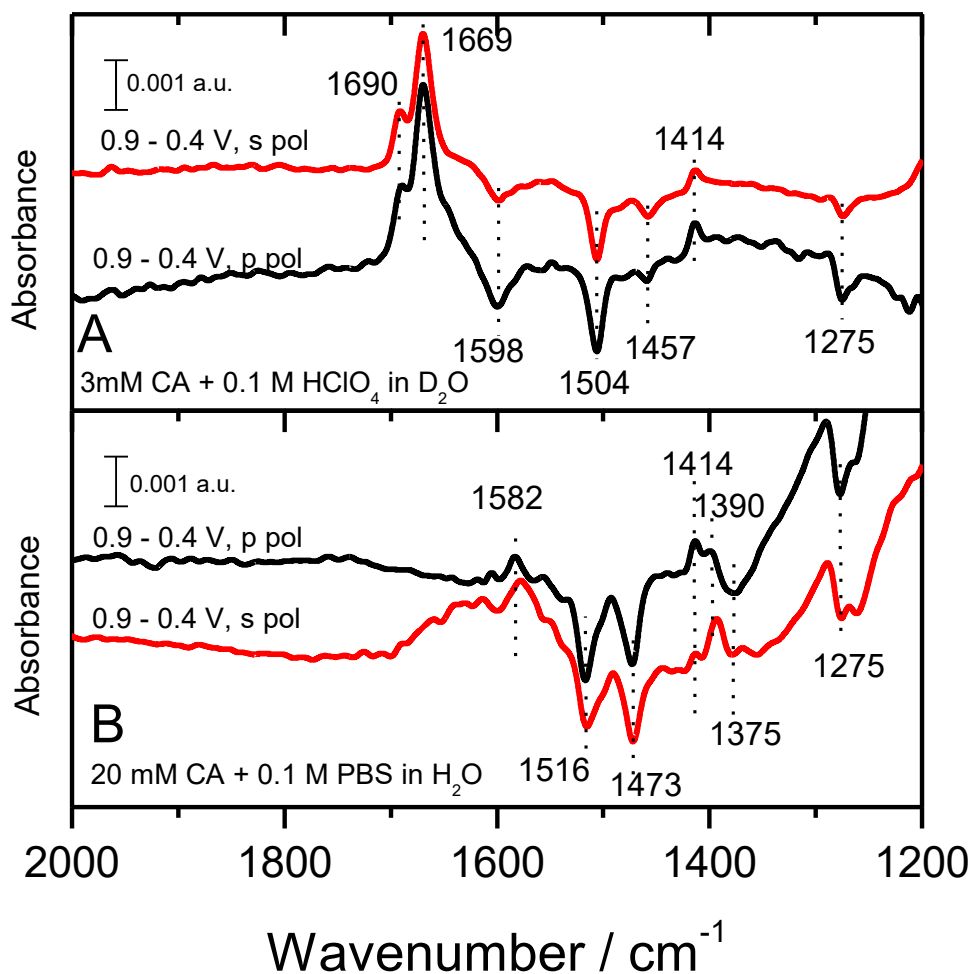


**Figure 7.** In situ absorbance spectra obtained for a Pt(111) electrode immersed in A) 3 mM CA + 0.1 M  $\text{HClO}_4$  solution in deuterium oxide water ( $\text{D}_2\text{O}$ ) and B) 20 mM CA aqueous 0.1 sodium PBS pH 7.2.  $E_{\text{ref}} = 0.4$  and  $E_{\text{sample}} = 0.9$  V. 200 interferograms were collected at each potential with a resolution of  $8 \text{ cm}^{-1}$  and p or s polarized light.

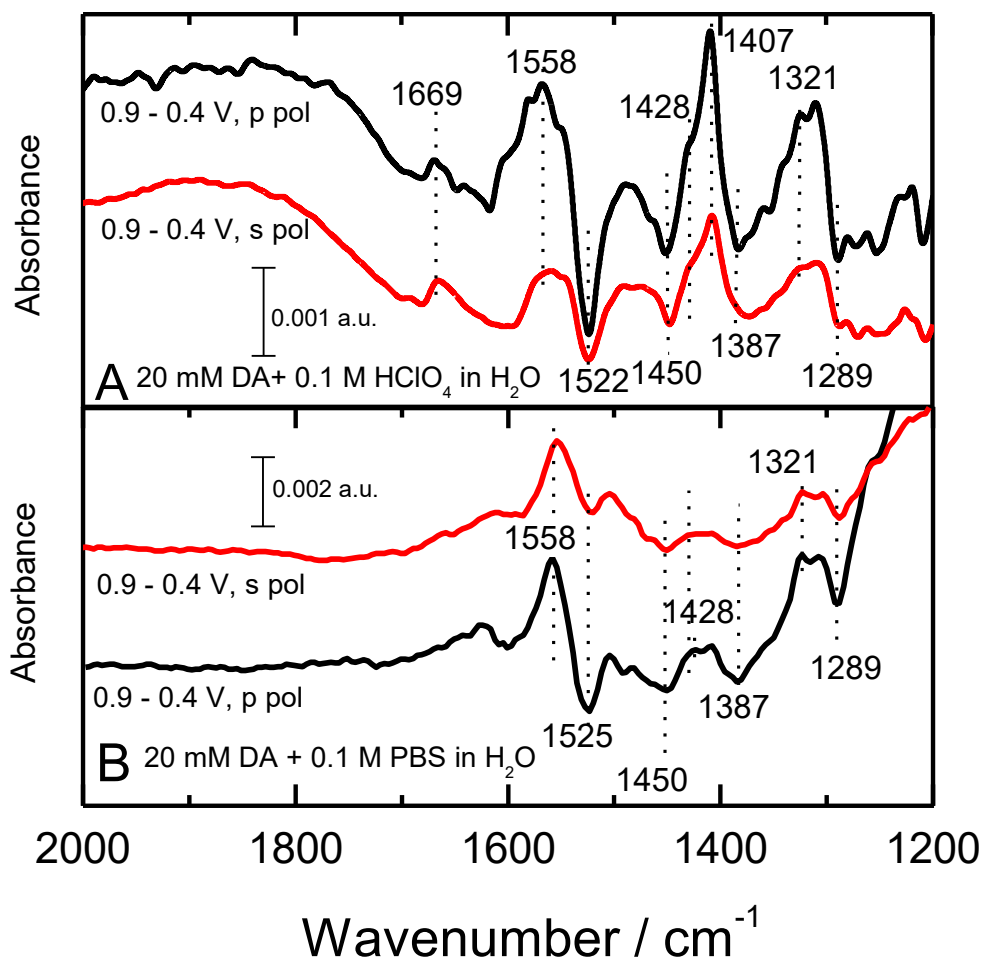


**Figure 8.** In situ absorbance spectra obtained for a Pt(111) electrode immersed in a 20 mM DA aqueous: A) 0.1M  $\text{HClO}_4$  and B) sodium PBS pH 7.2.  $E_{\text{ref}} = 0.4$  and  $E_{\text{sample}} = 0.9\text{V}$ . 200 interferograms were collected at each potential with a resolution of  $8\text{ cm}^{-1}$  and p or s polarized light.

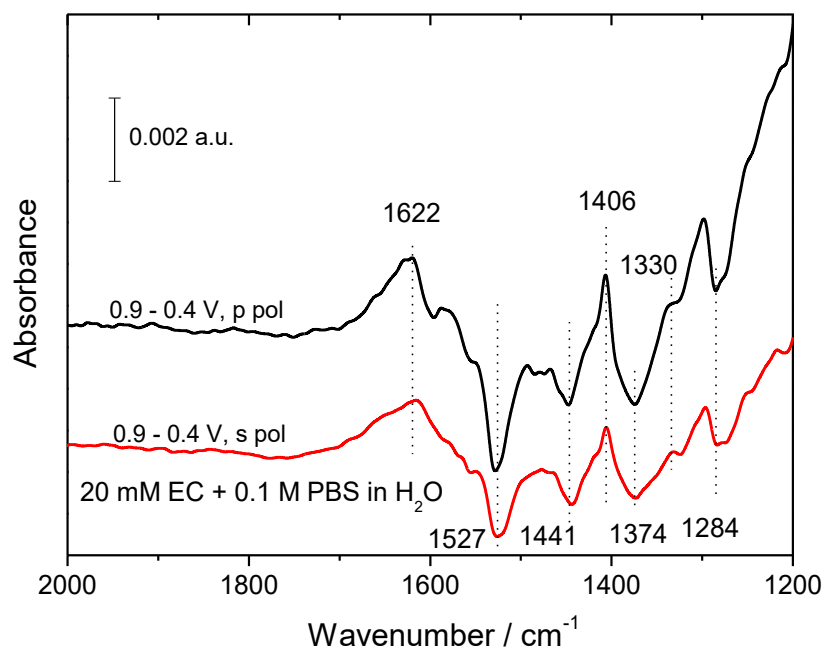


**Figure 9.** In situ absorbance spectra obtained for a Pt(111) electrode immersed in a 20 mM 4-EC aqueous 0.1 sodium PBS pH 7.2.  $E_{\text{ref}} = 0.4$  and  $E_{\text{sample}} = 0.9\text{V}$ . 200 interferograms were collected at each potential with a resolution of  $8\text{ cm}^{-1}$  and p or s polarized light.

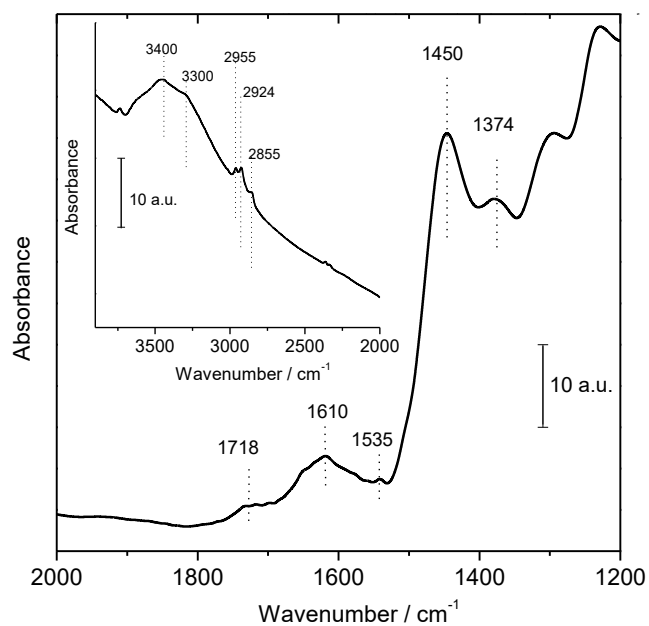


**Figure 10.** ATR of polydopamine adsorbed on a thin gold layer after potential cycling in a dopamine solution at pH 7.2, in dry conditions, 100 scans and 8 cm<sup>-1</sup>. Spectra were collected with p-polarized light.

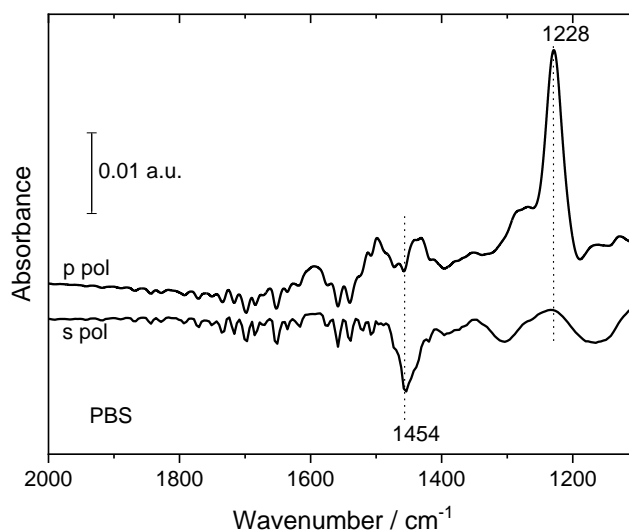


**Figure 11.** ATR of DA adsorbed on a thin gold layer after cycling in a sodium PBS (D<sub>2</sub>O) containing, 100 scans and 8 cm<sup>-1</sup>. p-polarized and s-polarized light, as indicated.

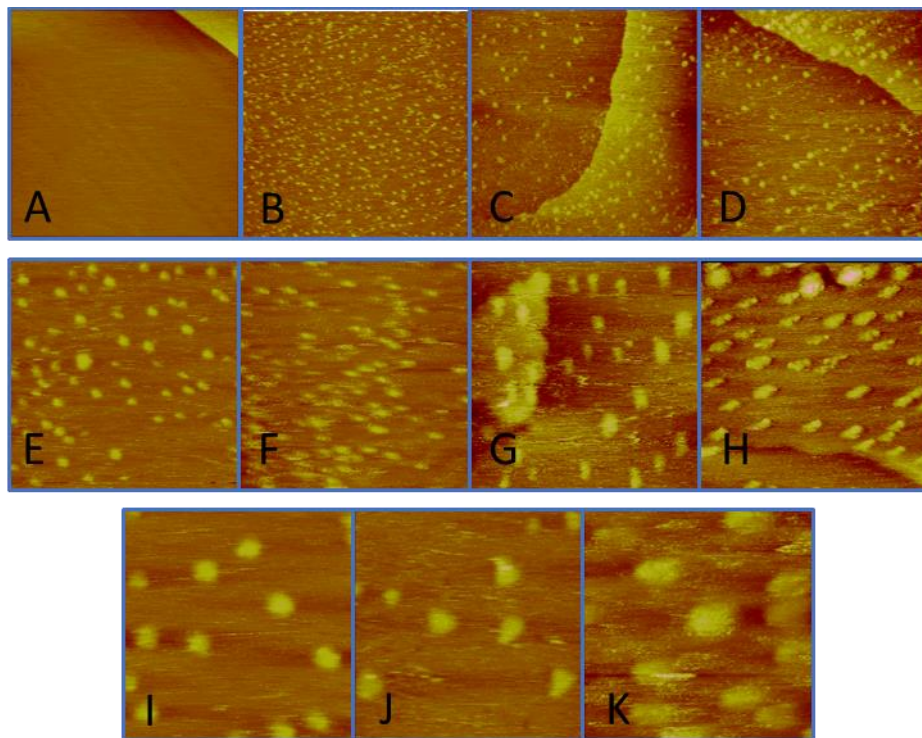


**Figure 12.** STM images of adsorbed DA or DA-derivative molecules over Au(111) in air under open circuit conditions. A) Au(111)-(1x1) substrate prior to dopamine adsorption. Scan Size: 100 x 100 nm<sup>2</sup>. B) to D) Scan size: 200 x 200 nm<sup>2</sup>: B) 2 cycles. C) 10 cycles and D) 50 cycles.. E) to H) Scan size: 100 x 100 nm<sup>2</sup>: E) 2 cycles. F) 10 cycles G) 25 cycles and H) 40 cycles. I) to K) Scan size: 50 x 50 nm<sup>2</sup> I) 2 cycles. J) 10 cycles and K) 25 cycles.  $E_{\text{bias}}$  100 mV.  $I_{\text{setpoint}}$ : 800 pA.



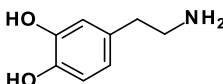
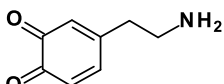
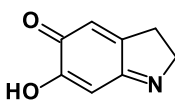
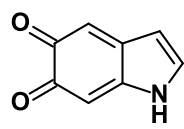
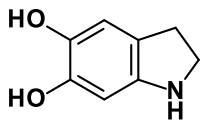
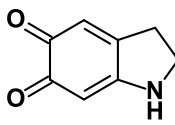
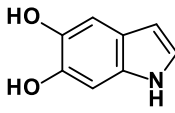
Tables:

Scan rate (mVs <sup>-1</sup> )	Cycle #	H <sub>2</sub> SO <sub>4</sub> (pH 0.65)		PBS (pH 7.2)		PBS (pH 10.8)	
		$\Delta E_p$ (mV)	$I_{red}/I_{ox}$	$\Delta E_p$ (mV)	$I_{red}/I_{ox}$	$\Delta E_p$ (mV)	$I_{red}/I_{ox}$
10	1	97 (108)**	0.27	157(146)**	0.78	*	*
20	1	117 (131)**	0.46	163(166)**	1.00	*	*
50	1 (10)	141(154)	0.25	196(231)	0.93	120(71)	0.03
100	1 (10)	145(175)	0.2	219(250)	0.43	99(77)	0.05
200	1 (10)	173(205)	0.23	*	*	106(99)	0.10
500	1 (10)	204(259)	0.25	324(448)	0.56	130(134)	0.28
1000	1 (10)	254 (308)	0.33	366(478)	0.71	167(171)	0.44

\* Not available

\*\*Cycle 5 (10 mVs<sup>-1</sup>) and Cycle 5 (20 mVs<sup>-1</sup>) in 0.5 M H<sub>2</sub>SO<sub>4</sub>. Cycle 3 (10 mVs<sup>-1</sup>) and Cycle 4 (20 mVs<sup>-1</sup>) in PBS (pH7.2)

**Table 1.** Peak potential separation ( $\Delta E_p$ ) and peak current ratio ( $I_{red}/I_{ox}$ ) for 1 mM catechol (CA) in H<sub>2</sub>SO<sub>4</sub> (pH 0.65), sodium PBS pH 7.2 and 10.8 on Pt electrodes.

Charge (0)	Charge (+2)	Charge (+4)	Charge (+6)
			
Dopamine	Dopaminequinone	Dopaminechrome	5,6-indolequinone
			
	Leucodopaminechrome 5,6-Dihydroxyindoline	5,6-Dihydroxyindoline quinone	
			
		Dihydroxyindole	

**Table 2.** Chemical structure of different oxidation products of DA.

Scan rate (mV/s <sup>-1</sup> )	Cycle #	H <sub>2</sub> SO <sub>4</sub> (pH 0.65)		PBS (pH 7.2)	
		$\Delta E_p$ (mV)	$I_{red}/I_{ox}$	$\Delta E_p$ (mV)	$I_{red}/I_{ox}$
10	1	70(90)**	0.35	145(82)**	0.09
20	1	78(97)**	0.57	164(126)**	0.15
50	1 (10)	102(117)	0.38	196(236)	0.36
100	1 (10)	126(137)	0.32	199(247)	0.36
200	1 (10)	183(191)	0.5	148(227)	0.27
500	1 (10)	201(208)	0.5	199(258)	0.46
1000	1 (10)	220(225)	0.5	219(298)	0.71

\*\*Cycle 4 (10 mVs<sup>-1</sup>) and Cycle 5 (20 mVs<sup>-1</sup>) in H<sub>2</sub>SO<sub>4</sub> 0.5M and PBS pH 7.2

**Table 3.** Peak potential separation ( $\Delta E_p$ ) and peak current ratio ( $I_{red}/I_{ox}$ ) for 1 mM DA in H<sub>2</sub>SO<sub>4</sub> (pH 0.65) and sodium PBS pH 7.2 on Pt electrodes.

Wavenumber (cm <sup>-1</sup> )	Assignment	References
H <sub>2</sub> O (D <sub>2</sub> O)		
Reduced (negative bands)		
(1598)	Ring C-C stretching	[47]
1516(1504)	Ring C-C stretching and CH bending	[17, 47, 48]
1473(1457)	Ring C-C stretching and CH bending	[17, 47, 48]
1275(1275)	C-OH stretching and CH ring bending	[17, 47, 48]
Oxidized (positive bands)		
1582(1670-1690)	C=O	[17]
1414(1414)		
1390(-)		

**Table 4:** Assignment of the main bands observed in the spectra for catechol in the oxidized and reduced state

Wavenumber (cm <sup>-1</sup> )	Assignment	References
Reduced (negative bands)		
1522	Ring C-C stretching	[49, 50]
1450	Ring C-C stretching and CH bending	[49, 50]
1289	C-OH stretching	[49, 50]
Oxidized (positive bands)		
1558	Aromatic C-C stretching (indoline quinone)	[49, 50]
1428	C=N <sup>+</sup> -C bond	[49, 50]
1407	Ring C-C stretching and CH bending	This work
1321	CH <sub>2</sub> bending	This work,

**Table 5:** Assignment of the main bands observed in the spectra for dopamine in the oxidized and reduced state

Wavenumber / $\text{cm}^{-1}$	Functional group Assignment
3400,3300	$\nu$ (N-H), $\nu$ (O-H)
2955,294, 2855	$\nu$ (C-H)
1718	$\nu$ (C=O)
1610	$\nu_{\text{ring}}$ (C=C)
1535	$\nu_{\text{ring}}$ (C=N)
1450	$\nu_{\text{ring}}$ (C=C)
1374	$\nu$ (C=N <sup>+</sup> -C)

**Table 6.** ATR bands of polydopamine deposited on a thin-gold layer electrode.

Number of Cycles	Scan Size/ nm	Size/ nm	Height/ nm
2	200	6.3	0.19
	100	6.1	0.19
	50	6.4	0.2
10	200	7.9	0.24
	100	7.3	0.25
	50	7.5	0.21
25	200	10.6	0.26
	100	10.2	0.29
	50	10.1	0.26
40	100	11.6	0.3
	100	11.8	0.3
50	200	12.9	0.39
	200	12.2	0.36

**Table 7.** Average size and height of the adsorbed DA derivatives spots for each different cyclic voltammetric cycles employed.

Supporting Information for:

**Analysis of Catechol, 4-Methylcatechol and Dopamine electrochemical reactions on different substrate materials and pH conditions.**

Sara Chumillas<sup>a</sup>, Tommi Palomäki<sup>b</sup>, Meng Zhang<sup>c</sup>, Tomi Laurila<sup>b</sup>, Victor Climent<sup>a\*</sup>, Juan Feliu<sup>a</sup>.

<sup>a</sup>Instituto Universitario de Electroquímica, Universidad de Alicante, Apt. 99, 03080 Alicante, Spain

<sup>b</sup>Department of Electrical Engineering and Automation, School of Electrical Engineering, Aalto University, PO Box 13500, 00076 Aalto, Finland

<sup>c</sup> State Key Laboratory of Physical Chemistry of Solid Surfaces, Department of Chemistry, College of Chemistry & Chemical Engineering, Xiamen University, Xiamen, 361005, P.R.China

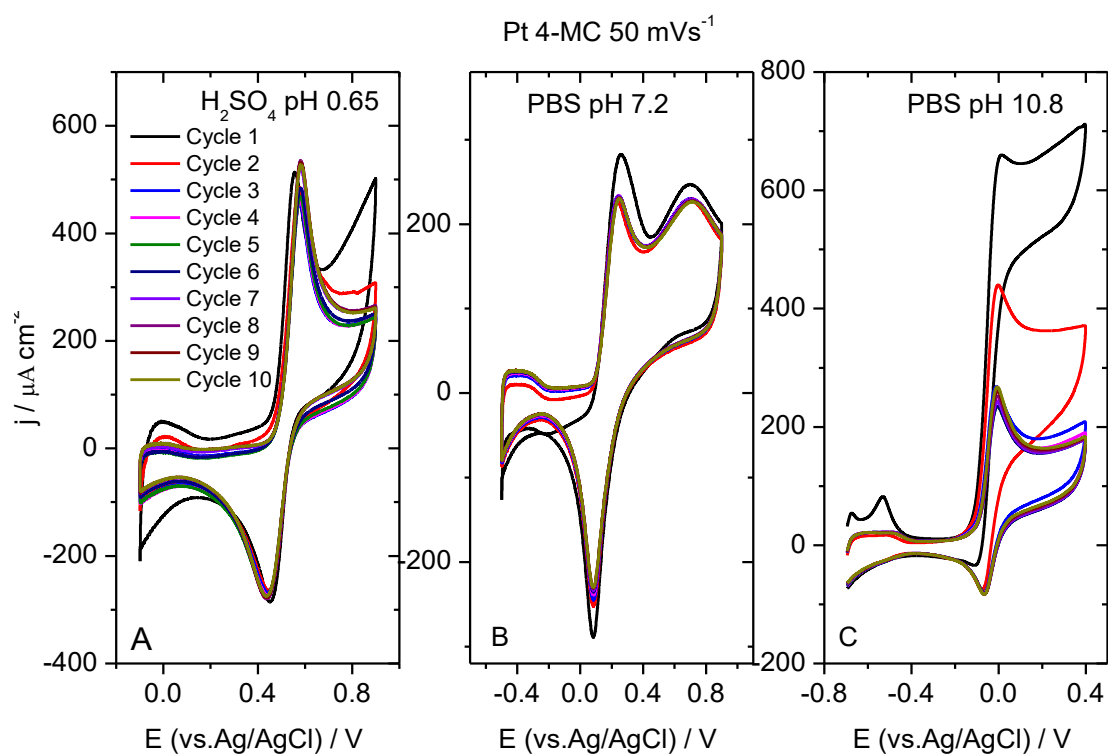


**Figure S1.** Cyclic voltammetric behavior of 4-MC on Pt in H<sub>2</sub>SO<sub>4</sub> pH (0.65) (A), PBS pH7.2 (B) and PBS pH 10.8 (C) at 50 mVs<sup>-1</sup>.

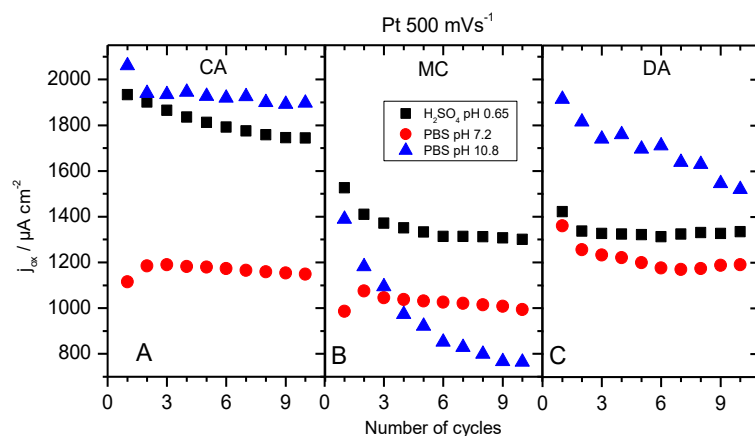


**Figure S2.** Oxidation current peak variation ( $j_{ox}$ ) versus number of cycles at  $500 mVs^{-1}$  on Pt for CA (A), 4-MC (B) and DA (C) in three different media:  $H_2SO_4$  pH 0.65 (black squares), sodium PBS pH 7.2 (red circles) and pH 10.8 (blue triangles).

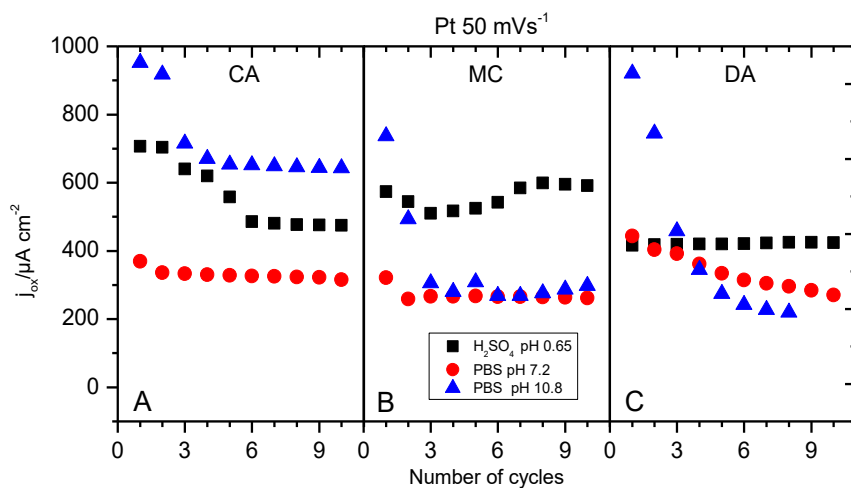


**Figure S3.** Oxidation current peak variation ( $I_{ox}$ ) versus number of cycles at  $50 mVs^{-1}$  on Pt for CA (A), 4-MC (B) and DA (C) in three different media:  $H_2SO_4$  pH 0.65 (black squares), sodium PBS pH 7.2 (red circles) and pH 10.8 (blue triangles).

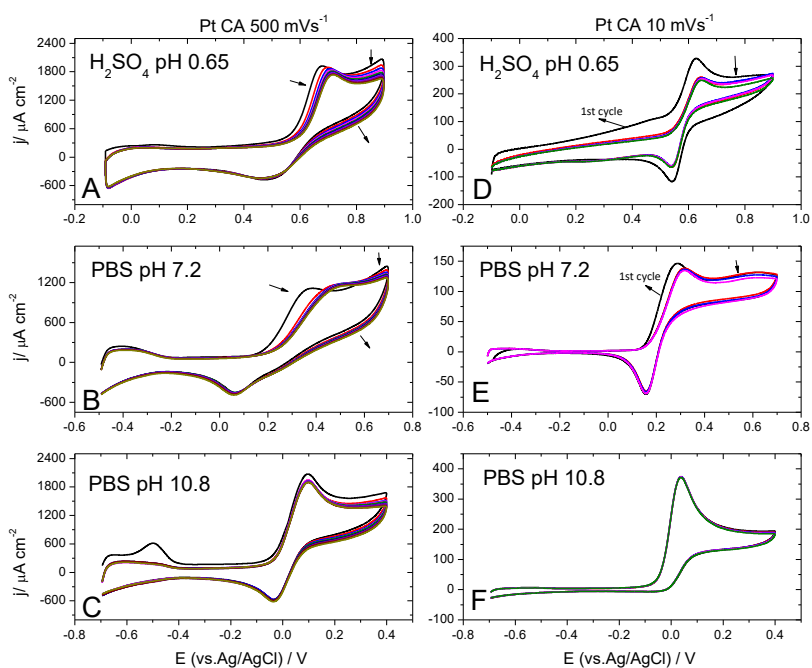


**Figure S4.** Cyclic voltammetric behavior for CA on Pt in  $\text{H}_2\text{SO}_4$  pH 0.65, sodium PBS pH 7.2 and pH 10.8 at  $500 \text{ mVs}^{-1}$  (A, B, C) and  $10 \text{ mVs}^{-1}$  (D, E, F).

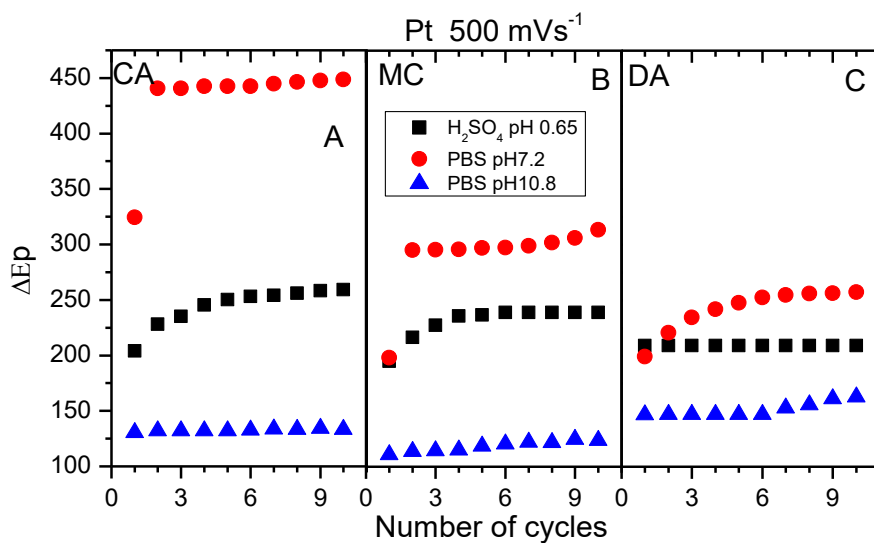


**Figure S5.** Peak potential Pt variation ( $\Delta E_p$ ) versus number of cycles at  $500 \text{ mVs}^{-1}$  for CA (A), 4-MC (B) and DA (C) for three different media  $\text{H}_2\text{SO}_4$  pH 0.65 (black squares), sodium PBS pH 7.2 (red circles) and pH 10.8 (blue triangles).

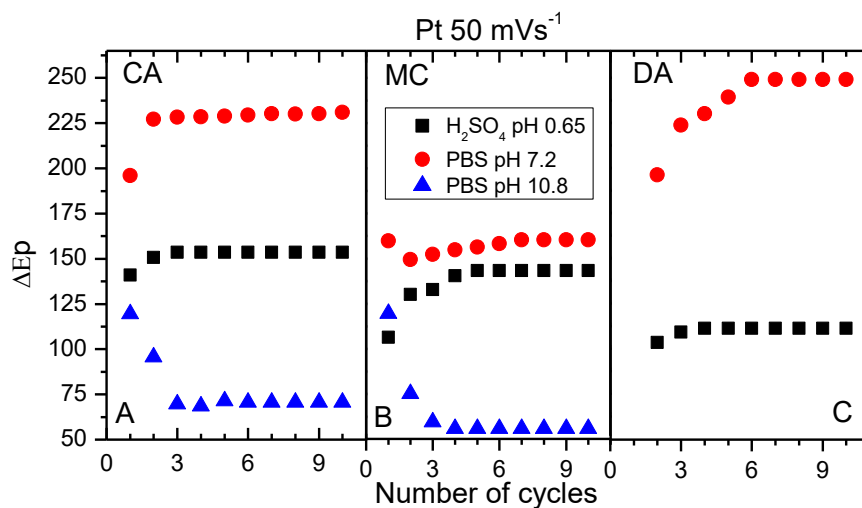


**Figure S6.** Peak potential Pt variation ( $\Delta E_p$ ) versus number of cycles at  $50 \text{ mVs}^{-1}$  for CA (A), 4-MC (B) and DA (C) in three different media:  $\text{H}_2\text{SO}_4$  pH 0.65 (black squares), sodium PBS pH 7.2 (red circles) and pH 10.8 (blue triangles).

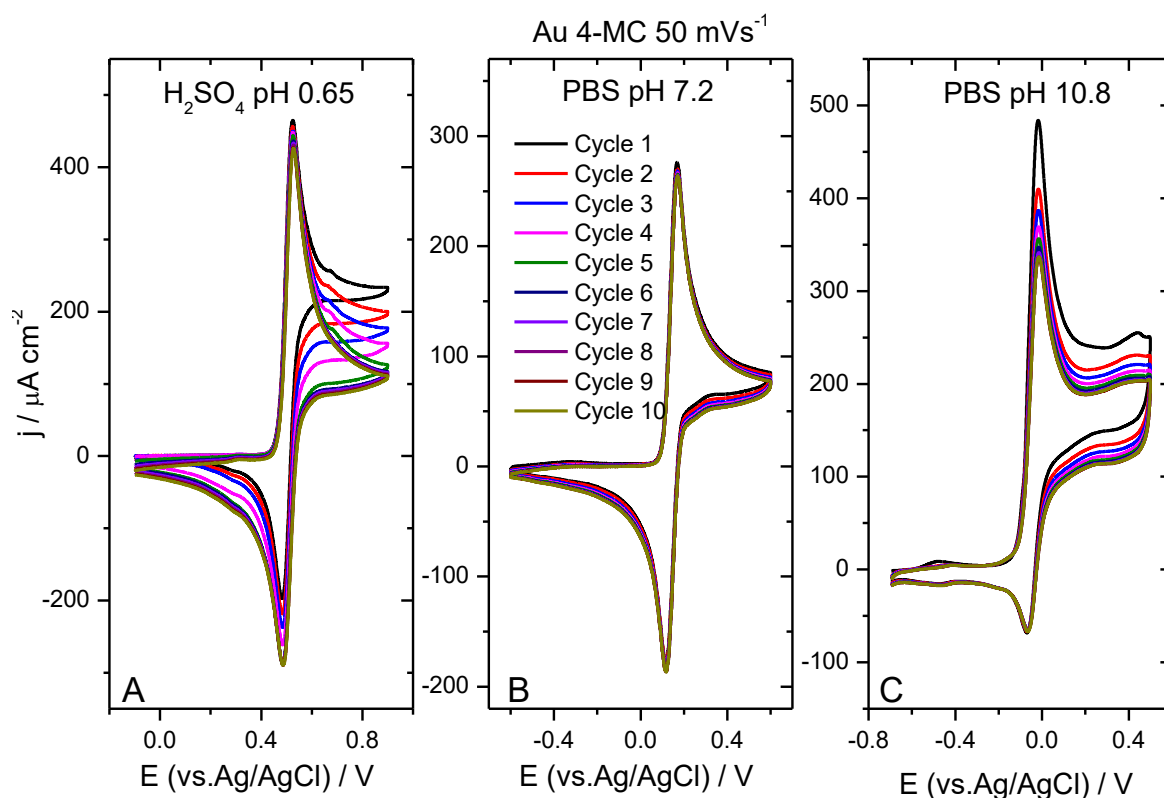


**Figure S7.** Cyclic voltammetric behavior of 4-MC on Au in  $\text{H}_2\text{SO}_4$  pH 0.65 (A), PBS pH 7.2 (B) and PBS pH 10.8 (C) at  $50 \text{ mVs}^{-1}$ .

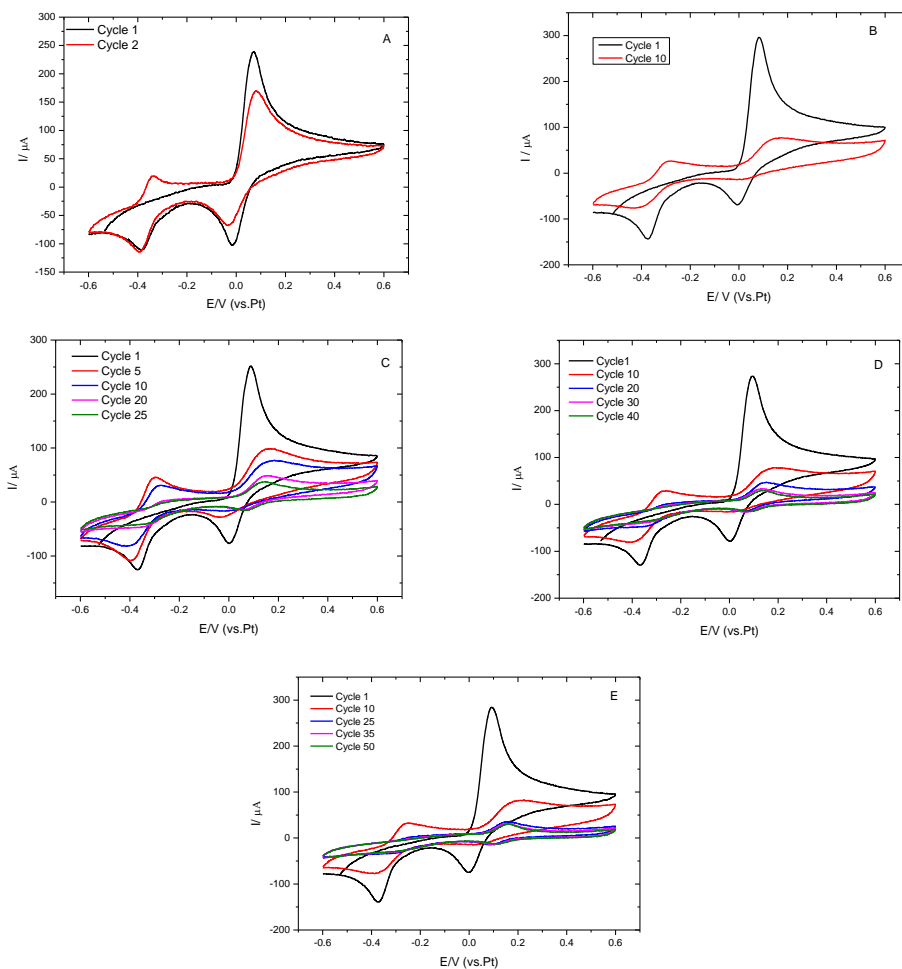


**Figure S8.** 1mM DA cyclic voltammetric behaviors on STM-Au(111) electrode in a sodium PBS, pH 7.2. Figures are classified depending on the total number of cycles recorded: A) 2, B) 10, C) 25, D) 40 and E) 50 cycles. Scan rate:  $50 \text{ mVs}^{-1}$ .

Tables

Scan rate (mVs <sup>-1</sup> )	Cycle #	H <sub>2</sub> SO <sub>4</sub> (pH 0.65)		PBS (pH 7.2)		PBS (pH 10.8)	
		$\Delta E_p$ (mV)	$I_{red}/I_{ox}$	$\Delta E_p$ (mV)	$I_{red}/I_{ox}$	$\Delta E_p$ (mV)	$I_{red}/I_{ox}$
10	1	71(101)**	0.52	94(96)**	0.72	*	*
20	1 (10)	93(102)**	0.46	107(116)	0.85	45(49)	0.09
50	1 (10)	106 (143)	0.56	160(161)	1	75(56)	0.17
100	1 (10)	150(184)	0.53	172(211)	0.63	61(71)	0.36
200	1 (10)	174(211)	0.30	192(241)	0.96	86(57)	0.43
500	1 (10)	195(239)	0.5	198(311)	0.86	111(124)	0.58
1000	1 (10)	219(258)	0.48	270 (342)	0.98	152(167)	0.65

\* Not available

\*\*Cycle 3 (10 mVs<sup>-1</sup>) and Cycle 4 (20 mVs<sup>-1</sup>) in 0.5M H<sub>2</sub>SO<sub>4</sub>. Cycle 3 (10 mVs<sup>-1</sup>) and Cycle 4 (20 mVs<sup>-1</sup>) in PBS (pH7.2)

**Table S1.** Peak potential separation ( $\Delta E_p$ ) and peak current ratio ( $I_{red}/I_{ox}$ ) for 1 mM 4-MC in H<sub>2</sub>SO<sub>4</sub> (pH 0.65), sodium PBS pH 7.2 and 10.8 on Pt electrodes

Scan rate (mVs <sup>-1</sup> )	Cycle #	H <sub>2</sub> SO <sub>4</sub> (pH 0.65)		PBS (pH 7.2)		PBS (pH 10.8)	
		$\Delta E_p$ (mV)	$I_{red}/I_{ox}$	$\Delta E_p$ (mV)	$I_{red}/I_{ox}$	$\Delta E_p$ (mV)	$I_{red}/I_{ox}$
10	1	41.3	0.11	48.1	0.25	*	*
20	1	43.3	0.19	49.4	0.40	*	*
50	1	45.4	0.33	58.6	0.48	50.9	0.02
100	1	45.7	0.49	68.3	0.59	66.6	0.074
200	1	52.1	0.51	73.2	0.65	73.57	0.15
500	1	54.3	0.51	100.6	0.66	93.8	0.25
1000	1	60.8	0.49	128.1	0.66	124.66	0.37

\* Not available

**Table S2.** Peak potential separation ( $\Delta E_p$ ) and peak current ratio ( $I_{red}/I_{ox}$ ) for 1 mM catechol (CA) in H<sub>2</sub>SO<sub>4</sub> (pH 0.65), sodium PBS pH 7.2 and 10.8 on Au electrodes.

Scan rate (mVs <sup>-1</sup> )	Cycle #	H <sub>2</sub> SO <sub>4</sub> (pH 0.65)		PBS (pH 7.2)		PBS (pH 10.8)	
		$\Delta E_p$ (mV)	$I_{red}/I_{ox}$	$\Delta E_p$ (mV)	$I_{red}/I_{ox}$	$\Delta E_p$ (mV)	$I_{red}/I_{ox}$
10	1	41	0.56	40.3	0.51	*	*
20	1	42.7	0.67	45.8	0.59	46.7	0.062
50	1	43.29	0.43	53	0.64	53.23	0.14
100	1	50.9	0.53	58.4	0.69	55.97	0.23
200	1	55.7	0.57	70.7	0.72	70.99	0.33
500	1	59.9	0.53	80.9	0.66	94.77	0.48
1000	1	66.7	0.50	106.5	0.63	108.83	0.56

\* Not available

**Table S3.** Peak potential separation ( $\Delta E_p$ ) and peak current ratio ( $I_{red}/I_{ox}$ ) for 1 mM 4-MC in H<sub>2</sub>SO<sub>4</sub> (pH 0.65), sodium PBS pH 7.2 and 10.8 on Au electrodes

Scan rate (mVs <sup>-1</sup> )	Cycle #	H <sub>2</sub> SO <sub>4</sub> (pH 0.65)		PBS (pH 7.2)	
		$\Delta E_p$ (mV)	$I_{red}/I_{ox}$	$\Delta E_p$ (mV)	$I_{red}/I_{ox}$
10	1	32**	0.28	83**	*
20	1	30**	0.43	86**	*
50	1	33	0.35	83 (267)	0.39
100	1	33	0.58	90 (244)	0.56
200	1	33	0.70	101 (208)	0.68
500	1	37	0.71	121 (195)	0.78
1000	1	42	0.70	141(149)	0.8

\* Not available

\*\*Cycle 4 (10 mVs<sup>-1</sup>) and Cycle 4 (20 mVs<sup>-1</sup>) in 0.5 M H<sub>2</sub>SO<sub>4</sub>, Cycle 3 (10 mVs<sup>-1</sup>) and Cycle 3 (20 mVs<sup>-1</sup>) in PBS (pH7.2),

**Table S4.** Peak potential separation ( $\Delta E_p$ ) and peak current ratio ( $I_{red}/I_{ox}$ ) of 1 mM DA in H<sub>2</sub>SO<sub>4</sub> (pH 0.65) and sodium PBS pH 7.2 on Au electrodes.

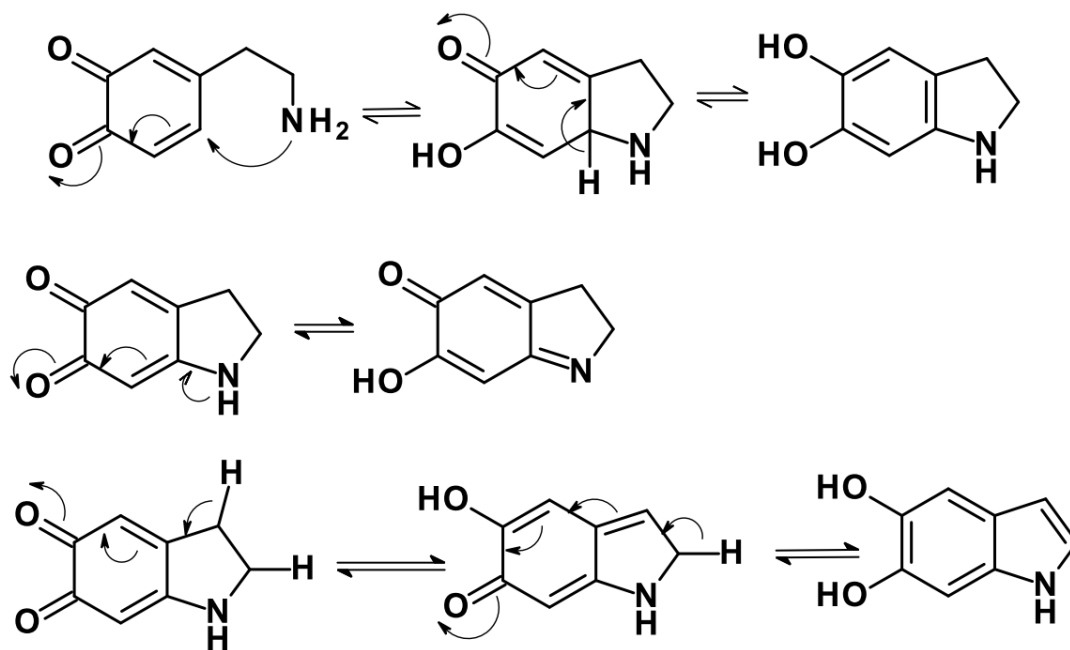
	Au			Pt			ta-C		
	$\Delta E_p$	$I_c/I_a$	fouling	$\Delta E_p$	$I_c/I_a$	fouling	$\Delta E_p$	$I_c/I_a$	fouling
<b>Catechol</b>									
<sup>(a)</sup> pH ↑	↔	↗↘	↑	↗↘	↗↘	↑	↗↘	↗↘	↑
v (mV/s) ↑	↑	↑	N.A	↑	↑	N.A	↑	↑	↓
<b>Methylcatechol</b>									
pH ↑	↔	↗↘	↑	↗↘	↗↘	↑	↗↘	↗↘	↑
v (mV/s) ↑	↑	↑	N.A	↑	↑	N.A	↑	↑	↓
<b>Dopamine</b>									
pH ↑	↑	<sup>(b)</sup> ↔	↑	<sup>(c)</sup> ↔	<sup>(b)(d)</sup> ↔	↑	↑	<sup>(b)(e)</sup> ↔	↑
v (mV/s) ↑	↑	↑	N.A	↑	↑	↓	↑	<sup>(f)</sup> ↑	<sup>(f)</sup> ↓

<sup>(a)</sup> Three pH values (0.65; 7.2; and 10.8), <sup>(b)</sup> No data at pH 10.8, <sup>(c)</sup> At low scan rates (< 100 mVs<sup>-1</sup>)  $\Delta E_p$  higher at elevated pH, <sup>(d)</sup> At low scan rates (< 100 mVs<sup>-1</sup>)  $I_c/I_a$  lower at elevated pH,

<sup>(e)</sup> At 50 mVs<sup>-1</sup>  $I_c/I_a$  is higher at pH 0.65 and at 500 mVs<sup>-1</sup> it is higher at pH 10.8

<sup>(f)</sup> At pH 0.65, there is no significant change

**Table S5.** General trends for the  $\Delta E_p$  (peak potential separation) ,  $I_c/I_a$  (cathodic and anodic intensity rate) and fouling dependence of CA, 4-MC and DA using different pH solutions and scan rates.



Scheme S1: DA and DA-derivative tautomeric relationships